European Commission

JRC SCIENCE AND POLICY REPORTS

Space Weather and Power Grids – A Vulnerability Assessment

Roberta Piccinelli, Elisabeth Krausmann

2014

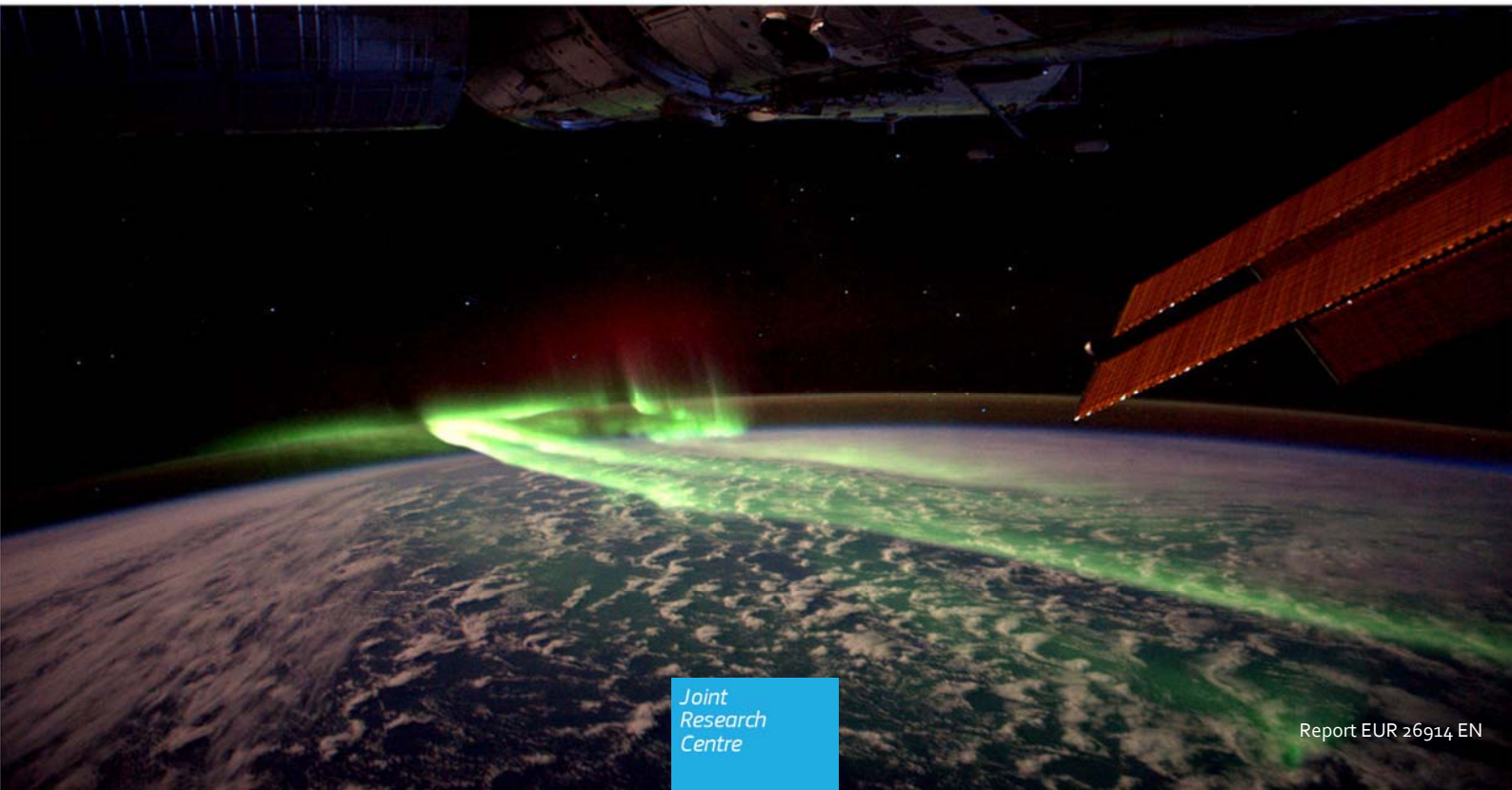

Joint Research Centre

Report EUR 26914 EN

European Commission
Joint Research Centre
Institute for the Protection and Security of the Citizen

Contact information
Elisabeth Krausmann
Address: Joint Research Centre, Via E. Fermi 2749, 21027 Ispra (VA), Italy
E-mail: elisabeth.krausmann@jrc.ec.europa.eu

https://ec.europa.eu/jrc

Image credits: Aurora Australis, as seen from the ISS (©ESA/NASA)

JRC92702

EUR 26914 EN

ISBN 978-92-79-43971-1

ISSN 1831-9424

doi:10.2788/20848

Luxembourg: Publications Office of the European Union, 2014

Abstract

Strong geomagnetic disturbances resulting from solar activity can have a major impact on ground-based infrastructures, such as power grids, pipelines and railway systems. The high voltage transmission network is particularly affected as currents induced by geomagnetic storms, so-called GICs, can severely damage network equipment possibly leading to system collapse. Therefore, increasing attention has been devoted to understanding the vulnerability of power grids to space weather conditions. In this study, we aim at analysing the vulnerability of power grids to extreme space weather. By means of complex network theory, we propose an analysis approach to understand how geomagnetically induced currents are driven through the power network based on its structural and physical characteristics. As a test network we used the Finnish power grid for which a study using network centrality measures was carried out to understand which components are the most critical for the system when exposed to an electric field of 1V/km. This information is helpful as the identification and ranking of critical components can help to identify where and how mitigation measures should be implemented to increase the system's resilience to space weather impact. We have also subjected the grid to varying angles of the electric field. In addition, we have carried out a scoping study adding load flow to the GICs induced in the system. The preliminary results suggest that the benchmark system can resist GICs induced from high intensity electric fields. Moreover, the simplified network seems more prone to collapse if the electric field is oriented northward. Work is underway to further validate and expand our approach with the aim to eventually carry out a risk assessment of space weather impact on the power grid at EU level.

Space Weather and Power Grids -

A Vulnerability Assessment

Roberta Piccinelli and Elisabeth Krausmann

Abstract

Strong geomagnetic disturbances resulting from solar activity can have a major impact on ground-based infrastructures, such as power grids, pipelines and railway systems. The high voltage transmission network is particularly affected as currents induced by geomagnetic storms, so-called GICs, can severely damage network equipment possibly leading to system collapse. The first accident of this kind occurred in Canada in 1989 where it took only 90 seconds for the entire Hydro-Quebec power grid to collapse during a geomagnetic storm. Since then, increasing attention has been devoted to understanding the vulnerability of power grids to space weather conditions.

In this study, we aim at analysing the vulnerability of power grids to extreme space weather. By means of complex network theory, we propose an analysis approach to understand how geomagnetically induced currents are driven through the power network based on its structural and physical characteristics. As a test network we used the Finnish power grid for which a study using network centrality measures was carried out to understand which components are the most critical for the system when exposed to an electric field of 1V/km. This information is helpful as the identification and ranking of critical components can help to identify where and how mitigation measures should be implemented to increase the system's resilience to space weather impact. We have also subjected the grid to varying angles of the electric field. In addition, we have carried out a scoping study adding load flow to the GICs induced in the system. The preliminary results suggest that the benchmark system can resist GICs induced from high intensity electric fields. Moreover, the simplified network seems more prone to collapse if the electric field is oriented northward.

Work is underway to further validate and expand our approach with the aim to eventually carry out a risk assessment of space weather impact on the power grid at EU level.

Table of Contents

1. Introduction

Geomagnetic disturbances produced by solar activity, also called space weather, can affect ground-based critical infrastructures, potentially causing damage to systems and resulting in failures and service disruptions. Among critical infrastructures, the long-distance, high-voltage power grids are particularly vulnerable to geomagnetic storms: effects may comprise both limited equipment failure and potential voltage instability resulting in uncontrolled cascading of the bulk power system (Krausmann et al, 2013; Schrijver and Mitchell, 2013).

The collapse of the Hydro-Québec transmission network during a geomagnetic storm in 1989 was a warning sign for the vulnerability of power grids to space weather events. The consequences of the Hydro-Québec blackout on the industrial production in a number of sectors also highlight the increased likelihood of significant domino effects in case of a power outage (Boteler, 2001).

Several studies have been dedicated to the assessment of the power grid's vulnerability to extreme space weather and to the investigation of the potential consequences of prolonged blackouts on society (NRC, 2008; Kappenman, 2010; JASON 2011; NERC, 2012). These studies focus on a potential major space weather impact on the North American transmission network and its components, and especially on high-voltage transformers. An extreme event, such as the 1859 Carrington event, is believed to be able to cause disruptions in the power grid that subsequently cascade to other critical infrastructures with a worst-case long-term recovery time for society of 4-10 years (NRC, 2008).

An extreme geomagnetic storm would encompass also a significant part of Europe (Pulkkinen et al, 2012). Various analyses of the vulnerability of the European power grid have considered reliability failures and intentional attacks (Brancucci et al, 2012; Rosas-Casals, 2007; Bompard, 2009) but hardly any information exists on the vulnerability of the European power grid to space weather events.

This study aims at identifying the vulnerability of the European power transmission grid with respect to extreme space weather by using complex network theory. We try to understand the spatial distribution and magnitude of GIC loading and the impact on grid operations potentially incurred. In a later step, this study will continue to estimate the impact of extreme space weather on society in Europe via the interdependencies of critical infrastructures with the power grid.

Section 2 presents a general overview of the physical phenomenon of geomagnetic storms and their impact on ground based critical infrastructures. In Section 3 we propose the vulnerability framework which will guide our analysis, and first results including a discussion are presented in Section 4. Conclusions and future work are discussed in Section 5.

2. Space weather and GICs

Space weather is a consequence of the interaction of the Sun, the Earth's magnetic field and the atmosphere. High-energy particles and radiation ejected from the Sun, once they reach the Earth, can cause temporary fluctuations of the geomagnetic field: these variations are called geomagnetic disturbances (GMDs). Transient fluctuations of sufficient severity are termed geomagnetic storms (GMSs).

Coronal mass ejections (CMEs), solar flares and radio bursts are the main phenomena connected with the formation of GMDs. CMEs are usually associated with large flares. If CMEs are Earth-directed, they interact with Earth's magnetosphere and cause geomagnetic storms that are observed on Earth one to six days after a flare or an eruption occurs on the Sun (FEN, 2013). GMSs, in turn, can create geomagnetically induced current (GICs) flows that can potentially affect the operation of power system equipment. Equipment impacted by previous storms include transformers, circuit breakers, generators and protective devices.

Several factors determine the degree to which a GMS affects the power system and its equipment. These include (NERC, 2012):

- Magnitude and orientation of the magnetic field
- Geomagnetic latitude
- Geology of the local area, including the electrical conductivity of the soil
- Proximity to an ocean or large water bodies
- Directional orientation, resistance and length of transmission lines
- Design of the power system and its equipment

GMSs can affect the components and the operation of power systems through a wide range of impacts. Effects with minor severity may be the tripping of electrical equipment or control malfunctions. Major GMSs may trigger voltage and reactive power fluctuations, local disruption of service, equipment failure and potential voltage instability that can potentially result in the uncontrolled cascading of the bulk power system.

2.1 Geomagnetic Storms (GMSs)

The sun continuously emits charged particles in all directions. This stream of mainly protons and electrons is called solar wind. CMEs are fast-moving bursts of plasma created by high-energy phenomena on the sun. They can reach the Earth in a matter of days, if oriented in the right direction, where the CME plasma then interacts with and perturbs the Earth's magnetosphere, a region in space where the motion of charged particles is determined by the Earth's magnetic field (Figure 1). Of significance for the formation of GMSs is the ionosphere, a part of the atmosphere where electric currents, or electrojets, periodically travel around the Earth (Püthe and Kuvshinov, 2013).

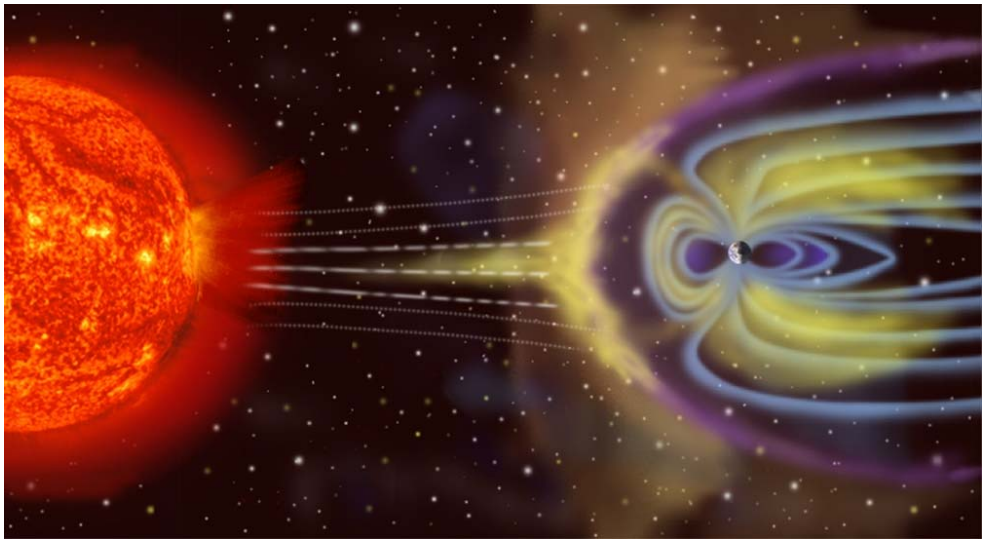

Figure 1. Schematic representation of solar wind particles interacting with Earth's magnetosphere. Size is not to scale (NASA, 2014).

Particularly relevant are the auroral electrojets which are large horizontal currents that flow in the auroral ionosphere following generally circular paths around the geomagnetic poles at altitudes of about 100 kilometers in an eastward (EEJ) or westward direction (WEJ), as shown in Figure 2 (INGV, 2014). Since the conductivity of the auroral ionosphere and its horizontal electric field are generally larger than that at lower latitudes, the auroral electrojet currents are particularly relevant for their strength and continuity.

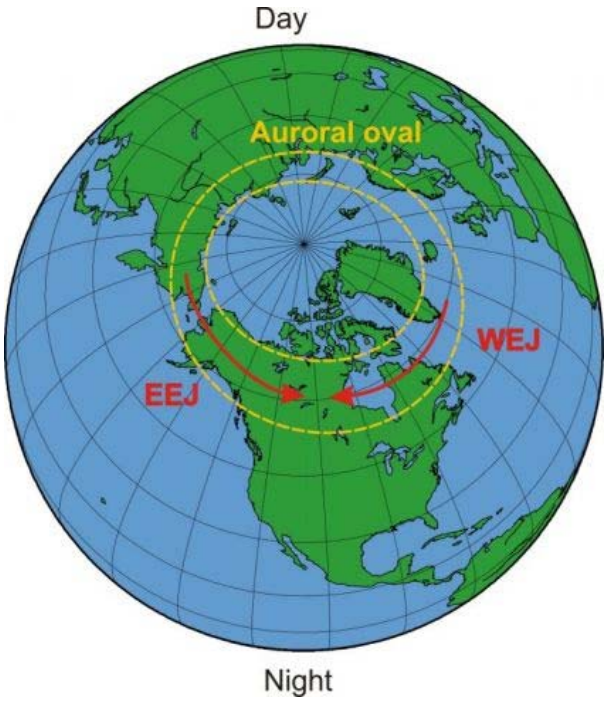

Figure 2. Representation of the East (EEJ) and West (WEJ) auroral electrojet (INGV, 2014)

When the geomagnetic activity is low, the electrojet would mostly be limited to the auroral oval. However, during periods with high geomagnetic activity, the electrojet expands to higher and lower latitudes and becomes stronger. This can result in geomagnetic field fluctuations, or GMDs. Severe transient fluctuations or GMSs are measured in nanoteslas (nT). The Earth's magnetic field at the poles is about 70 000 nT. During a severe storm, the fluctuation can be so strong so as to deflect compass needles.

A common scale used to indicate levels of geomagnetic activity are the K and A_k indices (SWPC, 2014). The K-index ranges from 0 to 9 and is related to the maximum fluctuations of the horizontal magnetic field variation over a three-hour interval. The maximum positive and negative deviations of the data recorded every minute over a 3-hour period are added to determine the total maximum fluctuation. These fluctuations may occur at any time during the 3-hour interval. The A_k index ranges from 0 to 400 and is a 24-hour index derived from 8 daily K indices. Values of K from 0 to 4 (and of A_k from 0 to 20) represent quiet geomagnetic activity, values from 5 to 6 (and of A_k from 30 to 50) represent a minor storm and a severe storm results in a K ranging from 7 to 9 (and of A_k from 100 to 400).

The solar activity approximately follows an 11-year cycle. Since 1755, when recording of the solar activity began, 24 cycles have been recorded. The current 24th cycle has begun in January 2009. The previous cycles 22 and 23 lasted from September 1986 to May 1996 and from May 1996 to December 2008 respectively.

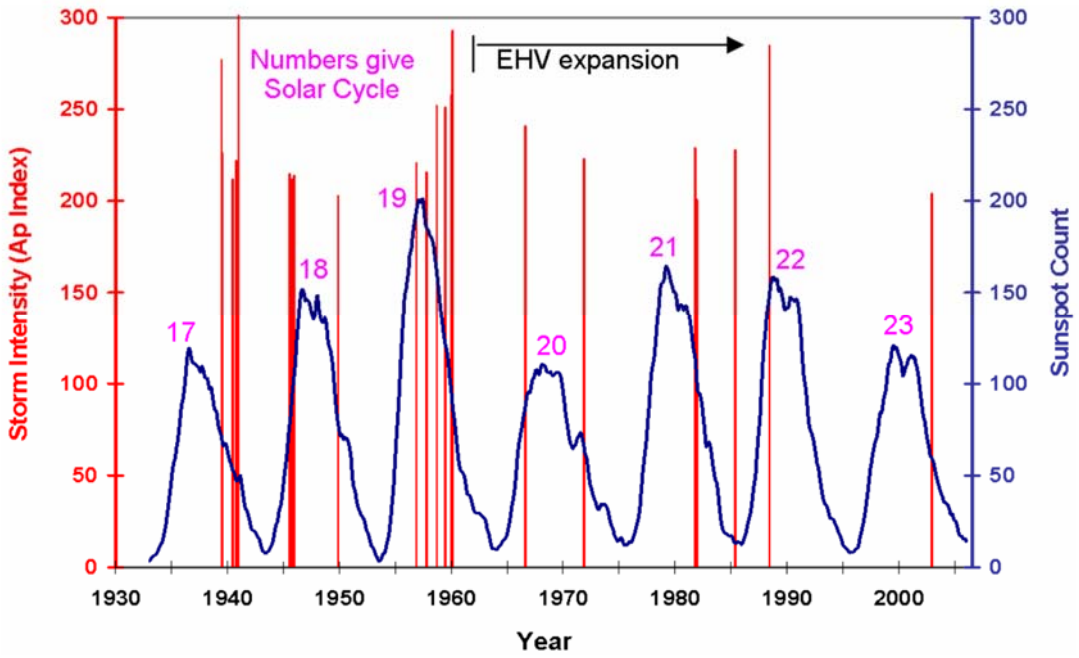

Figure 3. Sunspot cycles and the occurrence and intensity (using the A_p index) of geomagnetic storms (Kappenmann, 2010)

As shown in Figure 3, it appears that the geomagnetic activity is also cyclical, although it has to be stressed that a severe storm can occur at any time during a cycle, and not only around the peaks of sunspot activity. It should also be noted that not every solar event produces a GMD on Earth, which makes forecasting storms based on solar observation only very difficult. New forecasting capability is

based on missions by NASA and European Space Agency, which provides data on the space environment (NERC, 2012).
For electric utilities, however, it is more important to know the time derivative of the geomagnetic field over a few minutes because it is this value that is a key factor in calculating GICs (IEEE, 1993): for example, a rate of variation of 300 nT/min indicates a violent storm. Large values of K or A_k in general are not directly translatable into large GICs, since they depend on averages over a fixed period of time, and are thus only an indirect indicator of a GMD that can affect power systems.

2.2 Historical overview – Major GMSs of the past

The Carrington Event of 1859

The largest recorded magnetic storm occurred between August 27 and September 7, 1859 and it is known as the 'Carrington Event', after the British amateur astronomer who was the first to associate the storm with an intense solar flare 17.1 hours earlier. There were eyewitness accounts of auroras even at equatorial latitudes (JASON, 2011). The world's telegraph networks experienced severe disruptions, in some cases telegraph operators received electric shocks (NRC, 2008), and Victorian magnetometers were driven off the scale (BGS, 2014).

The 1921 Solar Storm

In May 1921, auroras were observed in Europe, across North America and far south at latitudes of 30-35 degrees (Silverman, 2001). This storm was reported to have "blown out fuses and injured electrical apparatus". Telegraph communications were disrupted in cities in the United States and some cables and telegraph lines to Alaska did not function during the storm (Solarstorms, 2014 and references of Newspapers herein).

The 1989 Québec Blackout

On 13 March 1989, a severe geomagnetic storm caused the entire Hydro-Québec transmission system to collapse (Boteler, 2001), resulting in a blackout that affected 6 million people. It took only 90 second for the grid to break down and more than 9 hours to restore power.

The blackout had ripple effects also on North American power system and utilities. One of the nuclear power plant transformers in Salem, New Jersey, suffered damage and had to be replaced.

The 2003 Halloween Solar Storms

The largest recent storms originate in 17 major solar flares that erupted on the sun between October 19 and November 5, 2003. Extensive effects on technological systems and human activities were reported. The most affected were spaced-based infrastructures: sensors and electronic devices of satellites were damaged and airline routes and schedules were significantly affected due to communication degradation and concerns about increased radiation exposure (NERC, 2012).

The electric power industry in North America experienced some effects, which include high levels of neutral current, capacitor trips, and some transformer heating.

The impacts were more significant in Northern Europe where an estimated GIC flow of 330 Amperes in a transformer in Southern Sweden caused a 130 kV line to trip, resulting in a 40 minutes blackout (NERC, 2012). No transformer issues were reported to be associated with the currents induced by the geomagnetic storm in Sweden.

2.3 Simulation of extreme GMSs

In order to simulate extreme GMS events, a number of factors that determine the geoelectric field need to be considered. The main factors are the effect of the ground conductivity structure and geomagnetic latitudes on the geomagnetic field amplitudes, as well as the temporal and spatial scales of the extreme geoelectric fields.

2.3.1 Ground conductivity structure

During geomagnetic storms, magnetic field variations produce an electric field that drives large electric currents through the ground and in conductor networks (Campbell, 1980; Boteler et al., 1998). Large power systems extend across different geological structures and the effect of conductivity changes needs to be accounted for when dealing with geomagnetic fields and GICs calculations.

Different techniques are available to develop ground conductivity models (Kappenman, 2010). On the one hand, descriptions of the local geology can be used to infer an average value of conductivity versus depth for the region of interest (Thomson et al, 2009; Pracser et al, 2012). Methods for modeling earth conductivity structures can be one- (1D), two- (2D) or three-dimensional (3D). Some models and methods are advantageous in terms of computation speed while others provide a better accuracy (Dong et al, 2013). Past experience has suggested that 1D Earth conductivity models are sufficient for the evaluation of the local electric field (Viljanen et al., 2012; Pracser et al, 2012; Kappenman, 2010). The general 1D model consists of a half-space, representing the ground, that is divided into N layers with the n-th layer having a resistivity ρ_n (or conductivity $\sigma_n = 1/ \rho_n$) and thickness z (Figure 4).

Mono-dimensional models only contain the variation of conductivity with depth and ignore any lateral variations. Discontinuity of the conductivity structure due to ground variations, for example near oceans, can be accounted for by using adequate boundary conditions.

On the other hand, actual measurements of geomagnetic and electric fields are available for certain regions of interest (Kappenman, 2010). Modern fluxgate magnetometers allow magnetic measures of the three-components of the magnetic field. In North America, The United States Geological Survey (USGS, www.usgs.gov) and the Geological Survey of Canada (GSC, www.nrcan.gc.ca/earth-science) operates the magnetic observatories. In Europe, the British Geological Survey (BGS, www.bgs.ac.uk) is one of the most active. Magnetic data are also available from these institutes through the InterMagnet international consortium website (www.intermagnet.org).

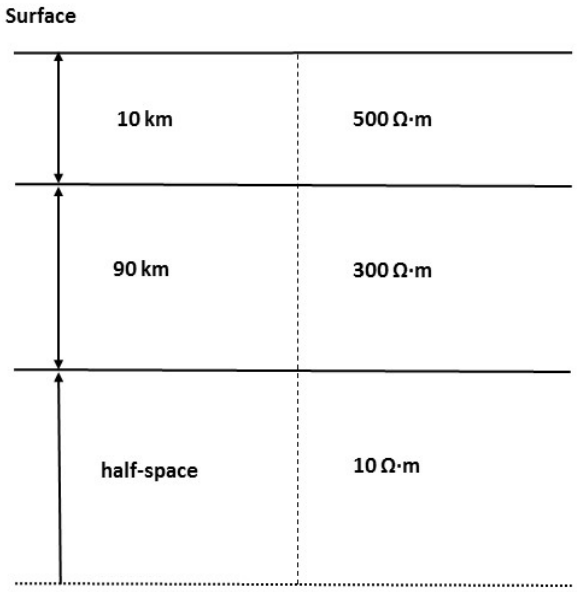

Figure 4. Mono-dimensional N-layered Earth model. Data are taken from Pracser et al (2012).

2.3.2 Temporal and spatial scale

The digital geomagnetic data can also be used to evaluate the rate of change of the magnetic field dB/dt. Figure 5 reproduces the percentage occurrences of dB/dt > 300nT/minute, derived from North American magnetic observatories. Since the probability variation with the geomagnetic latitude is smooth, the results were extrapolated along lines of constant geomagnetic latitude. The color grading extends from red, where the probability is higher, to yellow in those areas where the probability diminishes. A low probability for large GMD events is expected in most of North America and Central Europe (Molinski et al., 2000).

An alternative approach to the calculation of the electric fields is by means of a statistical analysis on the electric field values. Pulkkinen et al (2012) used 10-second samplings of geomagnetic data recorded from 1993 to 2006, thus covering a solar cycle period, to determine the electric field magnitude expected once in a 100 years. The two main results of this analysis are that the occurrence of large electric fields decreases with increasing amplitude (Fig. 6 left) and the peak electric fields shows a strong dependence on latitude (Fig. 6 right).

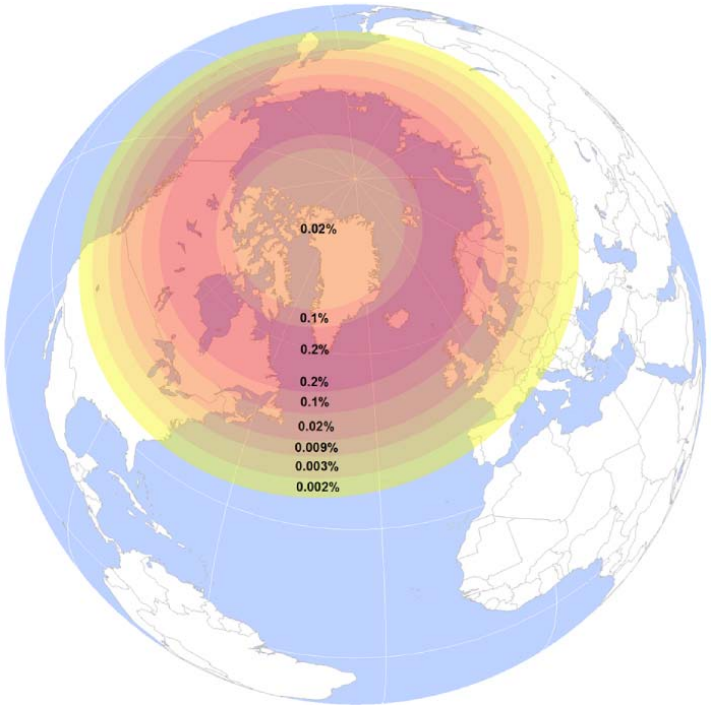

Figure 5. Map representing the probability of a significant geomagnetic storm, with a field change greater than 300nT/min (Rodrigue, 2014).

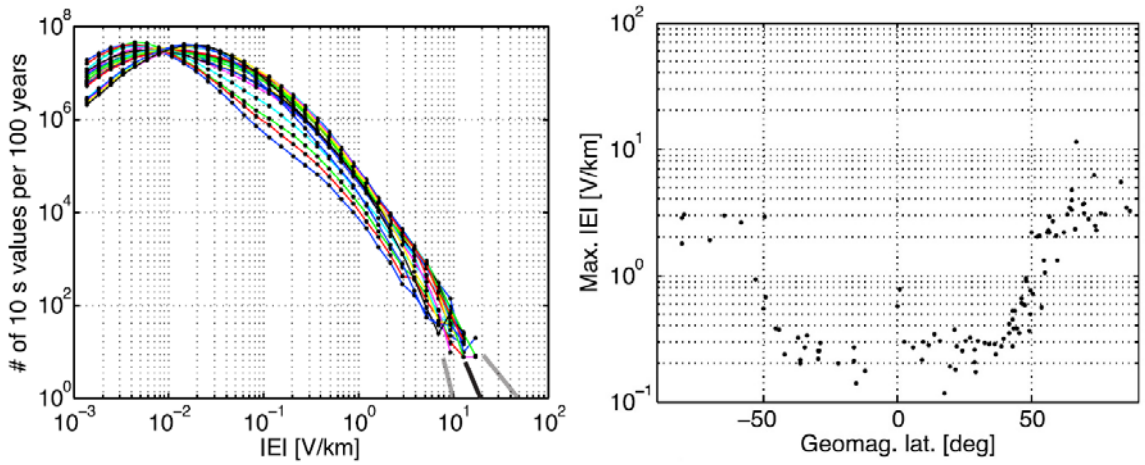

Figure 6. On the left, the statistical occurrence of the geoelectric field is represented: the different colors correspond to different IMAGE stations used in the computation. The thick black and grey lines represents the approximate extrapolation and the upper and lower boundaries, respectively. The maximum 100-year amplitude is estimated to be between 10-50V/Km. On the right, the geomagnetic latitude distribution of the maximum computed geoelectric field for the 2003 Halloween GMS is shown (Pulkkinen et al, 2012).

2.4 Space weather effects on power systems

The critical infrastructure that society has become most reliant on is the power grid. Power networks play a vital role in everyday life either as a standalone critical infrastructure providing electrical

power but also as a service provider to many other critical infrastructures that critically rely on the power grid.

GICs are quasi-DC currents that can cause numerous problems when entering the power grid. Transformers are particularly susceptible to GIC impact as they are not designed to handle the DC current. In fact, almost all power grid equipment and operations problems due to space weather arise from disturbed transformer performance, which is driven into half-cycle saturation by the GIC. As a consequence, the normally nearly linear relationship between input and output voltages and currents is shifted into a non-linear region. A number of secondary effects follow, such as increased reactive power consumption and the injection of even and odd harmonics into the power system. These harmonics cause even less compensating reactive power to be available, which can eventually lead to grid collapse (Molinski, 2002). Boteler (2001) notes that the situation is worse for power grids with long transmission lines, e.g. in the range of hundreds of kilometers, because longer lines have higher voltage support requirements.

The following sections briefly describe the main damage and failure modes associated with GIC loading in power grids.

Transformer saturation

Power transformers are used for stepping up voltage levels for electricity transport in transmission lines or reducing the voltage for electricity distribution to the customers. They use steel cores and are designed to be extremely efficient. As shown in Figure 7 (left), transformers usually operate in the linear range of their magnetic characteristic, which corresponds to an exciting current of only a few Amperes of AC. If GICs flow in the system, the operating point on the steel core saturation curve is shifted towards the nonlinear portion of the characteristic (Figure 7 right). Consequently, saturation occurs during one half of the cycle, causing a very high and asymmetrical exciting current (10-15% or more of the rated load current) to be drawn by the transformer (Ngnegueu et al, 2012).

Different transformer types are impacted differently by half-cycle saturation (Kappenman, 2010). Single-phase transformers, in particular, are more at risk than three-phase transformers because the quasi DC flux induced by the GIC can flow directly in the core. Furthermore, shell-type transformers are at greater risk than core-type transformers while autotransformers are particularly susceptible (Kappenman, 2010).

Reactive power losses

Transformers saturated by GIC loading have a higher reactive power consumption, which increases linearly with GIC magnitude (Albertson, 1973; Walling and Kahn, 1991). Single-phase transformers consume the largest amount of reactive power. A 90° voltage shift caused by the excitation current during saturation creates a reactive power demand from the power system. As a consequence there may be drops in system voltage and the stability margins may decrease significantly because additional reactive power is being consumed. The situation is exacerbated if voltage support devices trip during GIC events (Molinski, 2002) because of the injection of harmonics into the system.

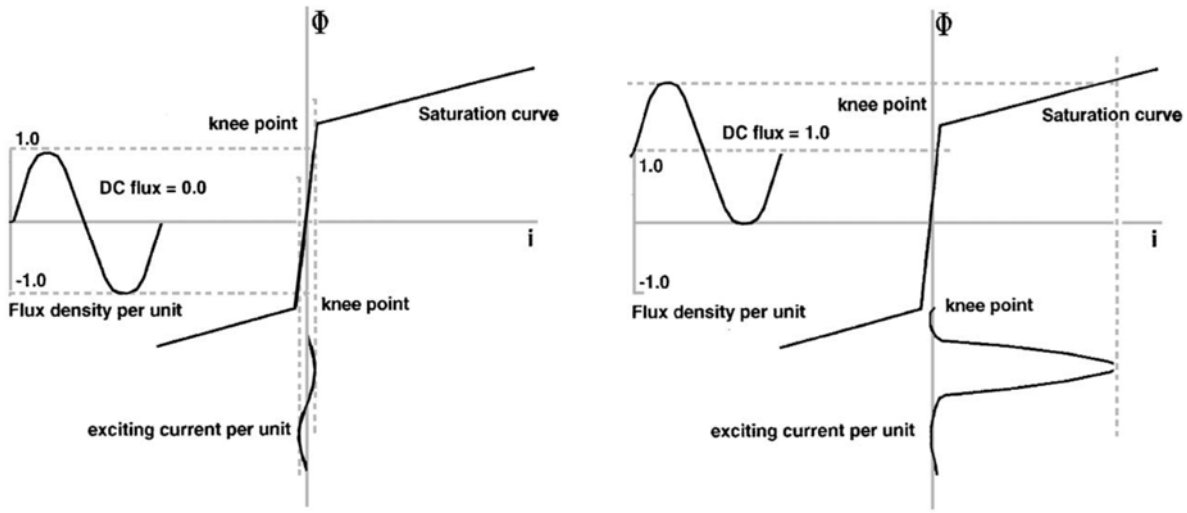

Figure 7. Relationship of exciting current and magnetic flux under normal operating conditions (left) and in the presence of GICs (right) (Molinski, 2002).

Harmonics

When a transformer is driven into half-cycle saturation, the exciting currents contain harmonics of various orders (fundamental, 2nd, 3rd, etc.), giving rise to complex current patterns. In case of very large GIC levels, the contribution of harmonics declines, especially at the higher orders, since the transformer is operating in a completely linear, although saturated, region of its magnetizing curve (Molinski, 2002). Power grids are generally designed to cope with odd harmonics (e.g. 3rd). However, they can be overwhelmed by even harmonics (e.g. negative sequence 2nd harmonic) because they are usually not expected during power operations (Molinski, 2002). False neutral overcurrent relay actuation may be the consequence. Moreover, harmonic currents can also cause additional series losses in e.g. circuit breakers and filter banks.

Transformer overheating

In case of transformer saturation most of the excess magnetic flux flows externally to the core into the transformer tank, where currents are created and localized tank wall heating with temperatures reaching 175°C can occur (Kappenman, 1996). If a transformer is repeatedly exposed to heating due to GIC loading, it can lead to cumulative insulation damage, accelerated ageing and eventually transformer failure (Koen and Gaunt, 2003). Unfortunately, in such cases it is usually not straightforward to relate cause and effect, so the real cause of transformer failure could be attributed to other reasons.

Generator overheating

Although no serious generator damage due to GMSs has been documented so far, there is at least theoretically some potential for damage (Molinski, 2002). Generators are usually shielded from direct GIC impact but they can still be affected by harmonics and voltage unbalance caused by transformer saturation. If harmonic currents enter the generator, excessive heating and mechanical vibrations can result. Moreover, the energy of the higher harmonic orders is concentrated near the

rotor surface which can also heat up and create a crack initiation site. As is the case for transformer heating, these phenomena may diminish the useful life of a generator, although the damage might not be immediately apparent and a potential failure at a later stage not necessarily attributed to GIC impact.

Protection relay tripping

In case of GIC flows, the harmonic content of the power system increases. With modern digital relays measuring the peak current value to monitor the status of the system, they are sensitive to tripping by harmonics. These false trips can then indirectly trigger a cascading failure of the power system. The relays' set current can be adjusted to accommodate the higher harmonics during GID impact and reduce the risk of false trips. However, this comes at the cost of lower protection levels (FEN, 2013).

Power systems increasingly depend on reactive power compensators and shunt capacitor banks for voltage control. Generally, shunt capacitors are grounded and have protection against unbalanced operation via neutral overcurrent relays. However, these capacitors banks are vulnerable to false trips during GMSs because of the capacitor's low impedance at the associated harmonic frequencies. Several power grid operators have upgraded or even replaced their neutral overcurrent unbalance protection to reduce the likelihood of false trips (IEEE, 1993).

Effects on communication systems for power grids

Geomagnetic storms also affect long-haul telephone lines, including undersea connections, and internet cables. The measurement and communication infrastructure directly used for power systems operation and control is expected to be relatively unaffected by GMSs, as the high-bandwidth lines in SCADA networks consist increasingly of optical fibers, which do not suffer the effects of electromagnetic disturbance (FEN, 2013). A potential system weakness lies in the use of Global Satellite Navigation System services (e.g. GPS) to obtain time stamps for, e.g. phasor measurements, as these space-based infrastructures would take the full brunt of the incoming solar storm and likely suffer a severe temporary service degradation.

2.5 Effects on other earthed critical infrastructures

2.5.1 Pipelines

Although there is controversy on the true impact of space weather on pipelines, there are indications that buried pipelines may suffer damage from steel corrosion due to GICs (Gummow, 2002; Pulkkinen et al, 2001; Pirjola et al, 2000). Corrosion is an electrochemical process occurring in pipelines at points where a current flows from the pipe to the soil. For example, a continuous DC current of 1 A flowing in a conductor for one year may cause a loss of about 10 kg of steel (Pirjola, 2012). To prevent or minimize corrosion, cathodic protection (CP) systems are implemented for pipelines. They keep the pipeline at a negative voltage of usually slightly below 1 V with respect to the soil. Pipe-to-soil voltages associated with GICs may exceed the CP voltage, which can render protection systems ineffective. Pipelines are covered with highly resistive coating which is preferred from a protection point of view. However, a high resistance also increases pipe-to-soil voltages implying larger harmful currents where defects are present in the coating (Pirjola, 2012).

Modeling of GICs in pipelines has evolved over the last thirty years. The first studies of Lehtinen and Pirjola (1985) presented theoretical calculations of GICs for the Finnish natural gas pipeline, with the assumption that the insulating coating of the pipeline was earthed at the cathodic protection stations. Viljanen (1989) presented a GIC study about the Finnish natural gas pipeline based on the simplified assumption that the pipeline is an infinitely long multi-layered cylindrical structure in a homogeneous medium.

An improvement in theoretical modelling is given by Boteler (1997) by incorporating the distributed-source transmission line theory (DSTL) into pipeline-GIC calculations. An extension is provided by Pulkkinen et al. (2001) which considers the branches of a pipeline network. In the DSTL theory, the pipeline is considered a transmission line containing a series impedance *Z* (or resistance due to the DC treatment) determined by the properties of the pipeline steel, and a parallel admittance *Y* associated with the resistivity of the coating (Boteler, 1997). The geoelectric field affecting the pipeline forms the distributed source. An important parameter, called the adjustment distance, is the inverse of the propagation constant γ defined by

$$\gamma = \sqrt{ZY} \tag{2.1}$$

Typical values of the adjustment distance of a real pipeline are tens of kilometers, with the exact values depending on the radius of the pipeline at a specific section. Usually, the adjustment distance ranges from about 20 km to about 60 km.

Pipelines are considered electrically long if their length significantly exceeds the adjustment distance; for electrically short pipelines the opposite is true. From a GIC point of view, electrically long pipelines exhibit a different behaviour than electrically short ones. For a long pipeline, the voltage decays exponentially at a distance comparable to the adjustment distance, when moving from either end of the pipeline towards the center where it is practically zero. Therefore, GIC flows between the pipe and the soil near the ends of a long pipeline, but the central parts are not critical regarding corrosion problems due to GIC Pirjola, 2012) On the other hand, for a short pipeline, the voltage changes linearly along the pipeline, and the current along the pipe is small when the ends are insulated from the Earth. Studies also show that the largest potential variations occur at discontinuities, such as at bends, insulating flanges and at the end of the pipeline.

2.5.2 Railways

Only very few studies exist on the potential impact of GICs on railway networks up till now: they mainly focus on anomalies in the operation of the signaling system. In 1982, a strong GMS affected the Swedish railway system. Between the nights of 13 and 14 July, apparently without reason, the traffic lights on the line turned red in a railway section of about 45 km length in South Sweden. The intense geoelectric field affected the relays connected to the rails inducing them to react as if a train occupied the rails (Wik et al, 2009).

From 2000 to 2005, 15 severe magnetic storms took place, and each of them had a response in the operation of the “Signalization, Centralization and Blockage (SCB)” system in the high-latitude parts of Russian railways. Also in these cases, the response of the network to the GMS caused false signals on the train occupation status of some parts of the railways (Belov et al., 2007; N. G. Ptitsyna, 2008; Eroshenko et al., 2010).

2.6 Calculation of GICs in power transmission networks

The calculation of GICs in conductors is usually carried out in two parts (Pirjola, 2002): first, the geoelectric field associated with the geomagnetic variation needs to be assessed. This part is purely geophysical and is independent of the technological system. Secondly, GICs due to the given geoelectric field are determined in the conductor system whose structure and features are known.

In the following, two possible scenarios will be introduced for the simulation of the geoelectric field: a first scenario in which the electric field is constant in magnitude but may vary in orientation and a second scenario in which the electric field can vary with time. The latter has been proposed by (Pulkkinen et al., 2012).

For the computation of GICs we follow the procedure proposed by Lehtinen and Pirjola (1985) which is explained in the next paragraphs.

A power system is a discrete grounded system with N nodes (earthing points). The GICs can be computed following the formula:

$$\mathbf{I^e} = \left(\mathbf{U} + \mathbf{Y^n Z^e}\right)^{-1} \mathbf{J^e} \tag{2.2}$$

where **U** is the unit matrix, and $\mathbf{Y^n}$ and $\mathbf{Z^e}$ are the network admittance matrix and earthing impedance matrix, respectively. The network admittance matrix $\mathbf{Y^n}$ is defined by

$$Y_{ij}^{n} = -\frac{1}{R_{ik}^{n}} (i \neq j) \tag{2.3}$$

and

$$Y_{ii}^{n} = \sum_{k \neq i} \frac{1}{R_{ik}^{n}} \tag{2.4}$$

where R_{ij}^{n} refers to the conductor line resistance between nodes i and j. The elements of the Nx1 column matrix $\mathbf{J^n}$ are defined by:

$$J_{i}^{e} = \sum_{j \neq i} J_{ij}^{n} \tag{2.5}$$

$$J_{ij}^{n} = \frac{V_{ji}}{R_{ij}^{n}} \tag{2.6}$$

$$V_{ji} = \int_{s_{ji}} \mathrm{E} \cdot \mathrm{ds} \tag{2.7}$$

The conductor line from node i to node j is denoted s_{ij} and **E** is the geoelectric field. Thus V_{ij} is the voltage affecting the line s_{ij}. The transmission line current from node i to node j can be solved from the equation:

$$I_{ij}^{n} R_{ij}^{n} = V_{ij} + \sum_{k,l} J_{l}^{e} \left(Z_{ik}^{e} - Z_{jk}^{e} \right) \left[\left(U + \mathrm{Y}^{n} \mathrm{Z}^{e} \right)^{-1} \right]_{kl} \tag{2.8}$$

3. Network vulnerability framework and risk assessment

Risk and vulnerability analysis are essential tools for proactive risk management. The meaning of the concepts and the interrelationship between them vary considerably between different disciplines. It is therefore important to define how these concepts are used for network vulnerability analysis. The sections below are a synthesis taken from Piccinelli (2013), Zio and Sansavini (2011), Zio et al. (2008), Zio and Piccinelli (2010) and Cadini et al. (2009). They provide an introduction to the vulnerability and complex network theory framework we applied, as well as the most important centrality measures used.

3.1 Vulnerability framework

The concept of the vulnerability of critical infrastructures is still evolving and a definition has not yet been unanimously established. Referring to the growing body of scientific literature on vulnerability, it emerges that the term vulnerability has different meanings when used in different contexts and by different authors (Bouchon, 2006). Disasters in the past showed that to understand risks a perception that is only centered on the concept of hazard is too limited. White (1974) notes that "a hazard of low intensity could have severe consequences, while a hazard of high intensity could have negligible consequences. The level of vulnerability makes the difference."

In the following, we adopt the definition of vulnerability as a susceptibility to disruption or destruction (inherent characteristic including resilience capacity) in the design, implementation, operation and/or management of an infrastructure system or its elements when exposed to a hazard or a threat (Haimes, 2006). This means that vulnerability is a state that exists within a system before it encounters a particular hazardous event (hazard independent, inherent vulnerability). This may depend on the structure of the system or on its operative states. Other definitions exist that view vulnerability as the amount of (potential) damage caused to a system by a particular hazardous event (hazard dependent).

Power networks are infrastructures that exhibit the characteristics of complex systems that require them to be analyzed from a holistic point of view which is challenging. The vulnerability analysis of these systems must take into account the potentially large number of spatially distributed components but also the diverse hazards and threats, including failures that the system can be subjected to. This consists of systematically identifying the possible states a system can be put into, given a specific strain, and estimating the impact associated with them. The two main outputs of vulnerability assessment are then 1) the identification of critical elements and 2) the quantification of system vulnerability indicators (Kröger and Zio, 2011).

There are three different analysis approaches, each covering different important aspects of vulnerability: *global vulnerability analysis*, *critical component analysis* and *geographical vulnerability analysis* (Johansson et al., 2011). These approaches are described in more detail in the following.

In a *global vulnerability analysis* a system is exposed to strains of different type and magnitude, and the negative consequences that result are estimated. As the magnitude of the strain increases, the performance of the system tends to degrade. Robust systems degrade slowly, whereas vulnerable systems might degrade quickly. In network analysis strains are represented by the removal of components whereas the magnitude of a strain corresponds to the number or fraction of

components removed. Different types of strains can be simulated by selecting different 'removal strategies' which can be random or targeted (Johansson et al., 2010).

Critical component analysis identifies the components that are the most critical and estimates the consequences of failure of single or sets of components to understand which system elements cause the largest negative consequences. In this analysis, all possible combinations of failures are evaluated which puts an upper limit to the feasible number of simultaneous failures that can be studied and hence it focuses on only relatively small magnitudes of strains. This is in contrast with global vulnerability analysis which aims to achieve a representative picture of the system's vulnerability for all magnitudes of strain and as a consequence, only a small sample of the possible states are evaluated (Johansson et al., 2010).

Geographical vulnerability analysis studies if geographic interdependencies exist that allow an external event, e.g., a hurricane, tornado, earthquake, explosion, etc., to damage several systems or components simultaneously. One type of geographical vulnerability analysis is the identification of critical geographical locations. In our approach, this is achieved by characterizing the strains through specific ground resistances values (Viljanen, 2012; Patterson and Apostolakis, 2007).

Each of the vulnerability analysis approaches described above provide only a partial view of the vulnerability of a system. If combined, they provide a more complete picture, which allows to obtain a more complete picture of a system's vulnerability (Johansson et al., 2011). In order to identify appropriate risk mitigation measures, the identified vulnerabilities must be combined with a hazard analysis in a comprehensive risk analysis that also includes determining likelihood estimations. However, the present report will only address the vulnerability part of risk.

Figure 8 shows the approach we used to model the space-weather impact on the power grid. We distinguish two models: the structural model, which captures the structural properties of the system by means of complex network theory modeling. This is the input to the functional model, which accounts for the physical properties and constraints given by the space weather effects on the system. Strains can be applied to each model: structural strains, which affect the structural properties of the system in terms of removal of components, and functional strains, which affect the physical properties of the system, e.g., increased loading or induced currents. In this report, we considered only functional strains.

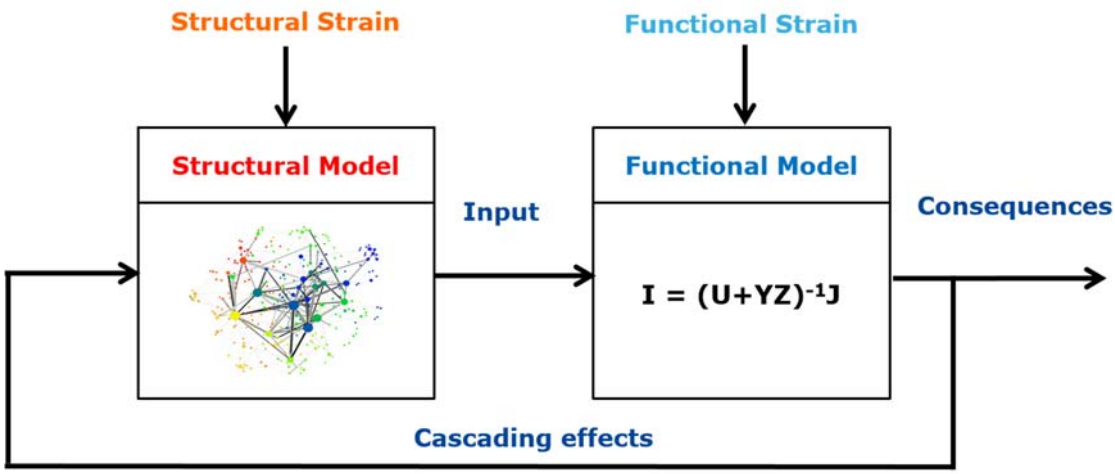

Figure 8. Approach used for modelling the space-weather impact on the power grid, with a structural and a functional part. The structural model represents a network consisting of nodes and edges. The functional model is represented by a linear equation (adapted from Johansson et al., 2013).

3.2 Complex network theory framework

Critical infrastructures (CIs), such as power grids, are complex systems of interacting components for which the actual structure of the interconnection is relevant (Albert et al, 2000). CIs can be modeled as hierarchies of interacting components. In a topological analysis, a CI is represented by a graph G(N, K), in which its physical components are mapped into N nodes (or vertices) connected by K edges (or arcs), which represent the links of physical connections among them.

Topological analysis based on classical graph theory can help to identify the relevant properties of the structures of a network system (Albert et al., 2000; Strogatz, 2001) by 1) highlighting the role played by its components (nodes and connecting arcs) (Crucitti et al., 2006; Zio et al., 2008), 2) making preliminary vulnerability assessments based on the simulation of faults (mainly represented by the removal of nodes and arcs) and the subsequent re-evaluation of the network topological properties (Rosato et al., 2007; Zio et al., 2008).

In the case of electrical power systems, the existing literature on vulnerability analysis follows a topological approach to identifying the critical components in the network (Albert et al., 2004; Crucitti et al., 2006; Zio et al., 2008). These analyses can help to identify the elements of structural vulnerability, i.e. network edges and nodes whose failure can induce a severe structural damage to the network through the physical disconnection of its parts. This kind of analysis is fast from a computational point of view and only requires information on the network topology.

Unfortunately, topological analysis cannot capture all the complex properties observed in a real infrastructure system. Consequently, the models need to be extended beyond pure structural topology (Boccaletti et al., 2006; Eusgeld et al., 2009). Through the identification of critical components, topological can highlight structural vulnerabilities. However, they are limited from the point of view of the functional vulnerability of the CI. More specifically, in real network systems the vulnerability characterization needs to be supplemented by modeling the dynamics of flow of the physical quantities in the network where physical laws and operational rules influence the flow. As a consequence, the interplay between structural and dynamic characteristics needs to be evaluated to provide information on the elements that are critical for the flow propagation process and on prevention and mitigation actions to reduce the risk of undesired effects. However, topological analysis is useful as a preliminary screening tool that requires minimal information but it is capable of identifying major vulnerabilities and guiding in-depth functional vulnerability analysis.

In addition to a complex topological structure, many real power networks exhibit significant physical inhomogeneities in the capacity and intensity of the connections: for example, there are different impedance and reliability characteristics of overhead lines in electrical transmission networks (Hines and Blumsack, 2008; Eusgeld et al., 2009). To capture the heterogeneity of real physical systems, weights can be assigned to each link of a network that measure the “strength” of the connection. In this way, the functional behavior of the CI is approximated in a generalized, but still simple, topological analysis framework. Topological, weighted or unweighted, analyses focus on the static structural properties of network interconnections and focus on the effects on vulnerability indicators caused by the removal of a certain percentage of nodes or links (Latora and Marchiori, 2005; Zio et al., 2008) or identifying the elements whose presence is critical with respect to the network connectedness (Cadini et al., 2009). Functional models exist that capture the basic realistic features of CI networks within a weighted topological analysis framework. This approach disregards the

representation of the individual dynamics of the power grid's elements. These models have helped to shed light on how complex networks react to faults and attacks under load flow.

Finally, complex network theory allows the consideration of dependencies and interdependencies among different CIs (Zimmermann, 2001; Duenas-Osorio et al., 2007; Johansson and Jonsson, 2009). In order to characterize how a threat could weaken, and possibly disrupt, the safe operation of an interconnected system, the relationship established via the connections linking the multiple components of the involved infrastructures needs to be modelled (Zio and Sansavini, 2011).

3.3 Centrality measures

Vulnerability analysis related to topology allows to address important questions related to the connectedness of nodes, shortest path lengths, geographical and regional specifics, etc. and to provide a reliable identification of the most critical connections, nodes or areas on which to focus a detailed analysis (Zio and Sansavini, 2011). However, caution needs to be exercised when relying on topological analysis only as its abstraction level is high. We therefore tried to reduce the gap between the very abstract topological analysis and the highly detailed (and computationally demanding) simulations of system behavior.

In order to quantify the structural importance of the network components, several so-called "centrality measures" have been introduced. Commonly, centrality measures provide an indication of the importance of a network element (arc or node), i.e., of the relevance of its location in the network with respect to a given network performance. Depending on the specific definition, a centrality measure describes the way in which a node interacts with the rest of the network. As such, it provides a measure that helps to rank and prioritise the importance of the nodes for network interaction. The term 'importance' qualifies the role that the presence and location of the element plays with respect to the average global and local connection properties of the whole network. Classical topological centrality measures are the degree centrality (Niemen, 1974; Freeman, 1979), the closeness centrality (Freeman, 1979; Sabidussi, 1966; Wasserman and Faust, 1994), the betweenness centrality (Freeman, 1979) and the information centrality (Latora and Marchiori, 2007). They rely only on topological information to determine the importance of a network element. It is important to note that critical groups of components can include elements that are not critical when considered individually. Therefore, the ranking of importance in the grid has to capture the most important component groups.

The **group degree centrality** (Everett and Borgatti, 1999), $C^D(g)$ of a group g in a network of N nodes, can be defined as the number of first neighbours of the group nodes, normalized over the number of non-group members:

$$C^D(g) = \frac{\sum_{i \in g} k_i}{N - \dim(g)} \tag{3.1}$$

where k_i is the degree of node i, in group g and dim(g) is the dimension of the group, i.e. the number of member nodes. A node that is connected with multiple group nodes is counted only once.

The **group closeness centrality** (Everett and Borgatti, 1999), $C^C(g)$ is based on the idea that a node can quickly interact with all the other nodes if it is easy accessible because close to all the others. If d_{ij} is the topological shortest path length (i.e., the number of connected arcs) between nodes i and j

(also called geodesics), the group closeness of a group g is the sum of such distances from the group to all vertices outside the group:

$$C^{C}(g)=\frac{N-\dim(g)}{\sum_{i\in g, J\in G} d_{ij}} \tag{3.2}$$

This measure is normalized by dividing the distance score by the number of non-group members. Consequently, larger numbers indicate greater centrality. When the group consists of a single node, the group closeness centrality becomes the individual node closeness centrality (Sabidussi, 1966; Freeman, 1979; Wasserman and Faust, 1994).

The distance from other nodes is one but not the only important property in a network of components. Of significance is also which nodes lie on the shortest paths among pairs of other nodes, because such nodes have control over the current flow in the network. Freeman (1979) defines the betweenness. In this definition, a node is central if it lies on several shortest paths among other pairs of nodes. If g is a subset of a graph, s_{ij} is the number of geodesics connecting i to j, and $s_{ij}(g)$ is the number of geodesics connecting i to j passing through g then the **group betweenness centrality** of g, denoted by $C^{B}(g)$ is given by (Everett and Borgatti, 1999):

$$C^{B}(g)=\frac{\sum_{i,j\in G, i<j} \frac{s_{i,j}(g)}{s_{i,j}}}{(N-\dim(g)-1)(N-\dim(g))} \tag{3.3}$$

where the sum is taken over all pair of nodes.

This measure is normalized by dividing it by the theoretical maximum value, which occurs for a group of a given size when the result of identifying all the group vertices (i.e., shrinking them to a single vertex) is a star with the group in the center.

The **global efficiency** of the graph representing the network is defined as (Latora and Marchiori, 2001):

$$E=\frac{1}{N(N-1)}\sum_{i,j\in G, i\neq j}\frac{1}{d_{ij}} \tag{3.4}$$

where $1/d_{ij}$ is the efficiency of the connection between nodes i and j in terms of the number of edges on the shortest path linking the two nodes. It relates the importance of an edge to the impact on the network transmission performance of losing the edges of a group and is hence a measure of importance of the group of edges removed (Crucitti et al., 2006). The relative variation of the global efficiency due to the removal of a group of edges is calculated as the difference between the global efficiency of the network with all the edges of the group removed and the global efficiency of the original network, normalized to the latter value.

The previous measure assume that flow is transmitted along geodesic paths in most networks, however, this is not the case (Stephenson and Zelen, 1989; Freeman et al, 1991), because the flow from one node of a network to another can take a circuitous route. For example, in network infrastructures flow is channeled through selected routes, following the specific operative rules and constraints which apply to the system. For the electric power network the flow obeys Kirchhoff's

laws. A realistic betweenness measure should include non-geodesic paths in addition to geodesic ones. To address this issue, a more sophisticated measure which includes the contributions from non-geodesic paths, has been proposed (Freeman, 1991).

If the generating sources and load nodes are known, the Ford-Fulkerson algorithm (Ford and Fulkerson, 1962) can be used to determine the maximum flow in the network, i.e., the largest possible total flow from sources to target nodes in the network, assuming that the flow at a node can be split among the edges in each node. The amount of flow through a node i when the maximum flow is transmitted from a source (s) to a target (t), averaged over all s and t is expressed by the **flow betweenness measure** (Freeman, 1991):

$$FC_i^B = \frac{\sum_{j=1}^{N}\sum_{k=j}^{N} m_{jk}(i)}{\sum_{j=1}^{N}\sum_{k=j} m_{jk}} \tag{3.5}$$

where m_{jk} be the maximum flow from node i to node k and $m_{jk}(i)$ is the maximum flow from node j to node k that passes through i. Each edge in the network can be envisaged as a transmission line carrying a current flow.

The flow betweenness is an indicator of the betweenness of nodes in a network in which a maximum flow is continuously pumped between all sources and targets. Clearly, the maximum flow needs to "know" the ideal route (or one of the ideal routes) from each source to each target. However, normally the flow does not follow the ideal path from source to target. This issue was considered in the **random walk betweenness** (Newman, 2005):

$$RWC_i^B = \frac{\sum_{i=1,s<t}^{N} I_i^{st}}{\frac{1}{2}N(N-1)} \tag{3.6}$$

where I_i^{st} is the current flowing through node i on the path from s to t. This measure is appropriate to a network in which the flow is transmitted more or less randomly until it finds its target, and it includes contributions from many paths that are not ideal. This measure is more physically detailed but it requires information on the system network connection pattern, the edges capacities, the values of the generating sources and loads, and an algorithm to evaluate the random walk of the flow through the network (Newman, 2005).

When considering the measurement of the connectivity of a node, the definition should consider the following three factors (Bompard, 2009): (i) the strength of connection in terms of the weights of the edge, (ii) the number of the edges connected with the nodes and (iii) the distribution of weights among the edges. The concept of entropy offers itself to define a degree that represents all the three factors mentioned above. First, p_{ij}, the normalized weight of the edge w_{ij} between nodes i and j, is considered, for each edge l_{ij} connecting nodes i and j:

$$p_{ij} = \frac{w_{ij}}{\sum_j w_{ij}} \tag{3.7}$$

Since $\sum_j p_{ij} = 1$ the **entropic degree** g_i of node *i* can be defined using entropy as:

$$g_i = \left(1 - \sum_j p_{ij} \log p_{ij}\right) \sum_j w_{ij} \tag{3.8}$$

The degree is a traditional concept in graph theory that is widely applied to the analysis of complex networks. Bompard, (2009) notes that the entropic degree may be a good replacement for weighted network models used for power grids, gas pipelines, water ducts and transportation. In the case of power grids, the entropic degree can provide a direct quantitative measurement of the importance of buses. This gives an indication of where additional resources should be directed to increase protection.

4. Power Grids and Geomagnetically Induced Currents (GICs)

4.1 Case-study: benchmark power grid

Studies on GIC assessment have been proposed in the scientific literature for different power grid models: (NERC 2012; Horton et al, 2012; Pirjola, 2009)

Following the suggestion of Pirjola (2009) we adopt, as benchmark model, the Finnish 400-kV transmission power grid, as it was in its configuration from October 1978 to November 1979. The network, depicted in Figure 9, consists of 17 stations and 19 transmission lines: the numbers of stations and transmission lines are high enough to allow a meaningful analysis but is not too large to complicate computation and analysis. Each station is assumed to include a transformer.

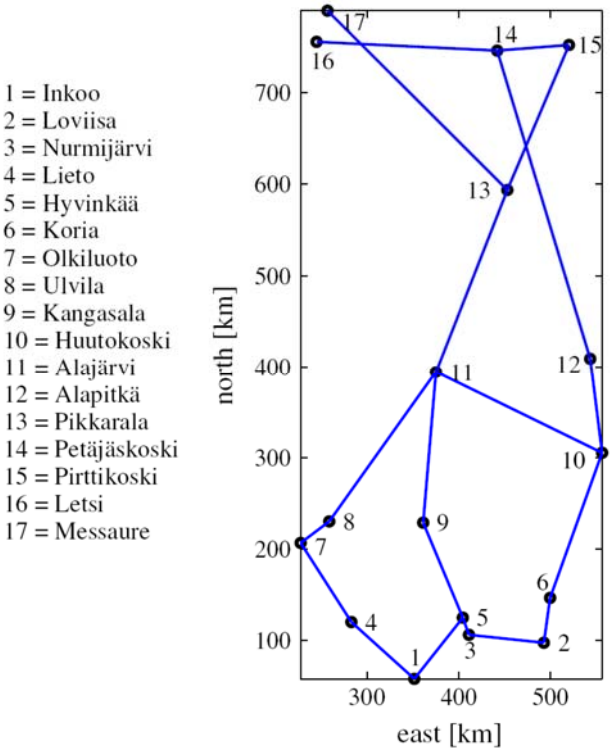

Figure 9. Schematic map of the Finnish 400 kV power grid in 1978 – 1979. Transmission lines are approximated by straight lines, while stations are represented by nodes. Each node is assumed to represent a transformer (taken from Viljanen et al., 2012).

Data of the network have initially been proposed by Lehtinen and Pirjola (1985). The coordinates and earthing resistances of the stations and the resistances of the transmission lines are given for the sake of completeness s in Tables I and II, respectively. The earthing resistances listed in Table I include the effects of the station earthings and the transformers. The earthing resistances of stations 16 and 17 are set equal to zero to account for the connection to the Swedish 400-kV network. Thus, the currents at nodes 16 and 17 include currents that flow between the Finnish and the Swedish systems and do not account for earthing GICs (Pirjola, 2009).

Station	Coordinates [km]		Earthing Resistance [Ω]
	East	North	
1 = Inkoo	351.44	58.17	0.43
2 = Loviisa	492.79	97.60	0.36
3 = Nurmijärvi	411.06	106.25	0.66
4 = Lieto	282.69	120.19	0.60
5 = Hyyinkää	404.33	125.00	0.47
6 = Koria	499.52	146.63	0.45
7 = Olkiluoto	227.40	206.73	0.33
8 = Ulvila	258.65	230.29	0.64
9 = Kangasala	361.06	228.85	0.86
10 = Huutokoski	556.25	305.29	0.57
11 = Alajärvi	375.00	394.23	0.98
12 = Alapitkä	543.27	409.13	1.14
13 = Pikkarala	452.88	593.75	0.70
14 = Petäjäskoski	441.83	746.15	0.47
15 = Pirttikoski	520.19	752.40	0.95
16 = Letsi	244.71	755.77	0
17 = Messaure	256.73	789.90	0

Table I. List of the stations (nodes) of the Finnish 400-kV transmission power grid shown in Fig. 9. The east (x) and north (y) coordinates and the total earthing resistances of each node are also shown (Lehtinen and Pirjola, 1985).

Line Number	Station A	Station B	Line Resistance [Ω]
1	1 = Inkoo	4 = Lieto	0.59
2	1 = Inkoo	5 = Hyyinkää	0.65
3	2 = Loviisa	3 = Nurmijärvi	0.58
4	2 = Loviisa	6 = Koria	0.33
5	3 = Nurmijärvi	5 = Hyyinkää	0.076
6	4 = Lieto	7 = Olkiluoto	0.59
7	5 = Hyyinkää	9 = Kangasala	1.04
8	6 = Koria	10 = Huutokoski	1.36
9	7 = Olkiluoto	8 = Ulvila	0.27
10	8 = Ulvila	11 = Alajärvi	1.98
11	9 = Kangasala	11 = Alajärvi	1.47
12	10 = Huutokoski	11 = Alajärvi	1.88
13	10 = Huutokoski	12 = Alapitkä	0.98
14	11 = Alajärvi	13 = Pikkarala	0.96
15	12 = Alapitkä	14 = Petäjäskoski	3.20

16	13 = Pikkarala	15 = Pirttikoski	1.46
17	13 = Pikkarala	17 = Messaure	2.89
18	14 = Petäjäskoski	15 = Pirttikoski	0.71
19	14 = Petäjäskoski	16 = Letsi	1.70

Table II. Transmission lines between stations A and B and resistances of the Finnish 400-kV power grid shown in Fig. 9 (Lehtinen and Pirjola, 1985).

The first aim of the vulnerability analysis is to understand if and how the structure of the network influences the diffusion of GICs in the system. Since the voltage in the transmission lines is obtained by integrating the horizontal geoelectric field along the path defined by the conductor line that connects two stations, it is noteworthy to look at the line lengths. The Finnish 400-kV transmission network shows a broad distribution of line lengths (Figure 10): two lines measure less than 50 km while the longest line measures 352 km. The average length is 147 km.

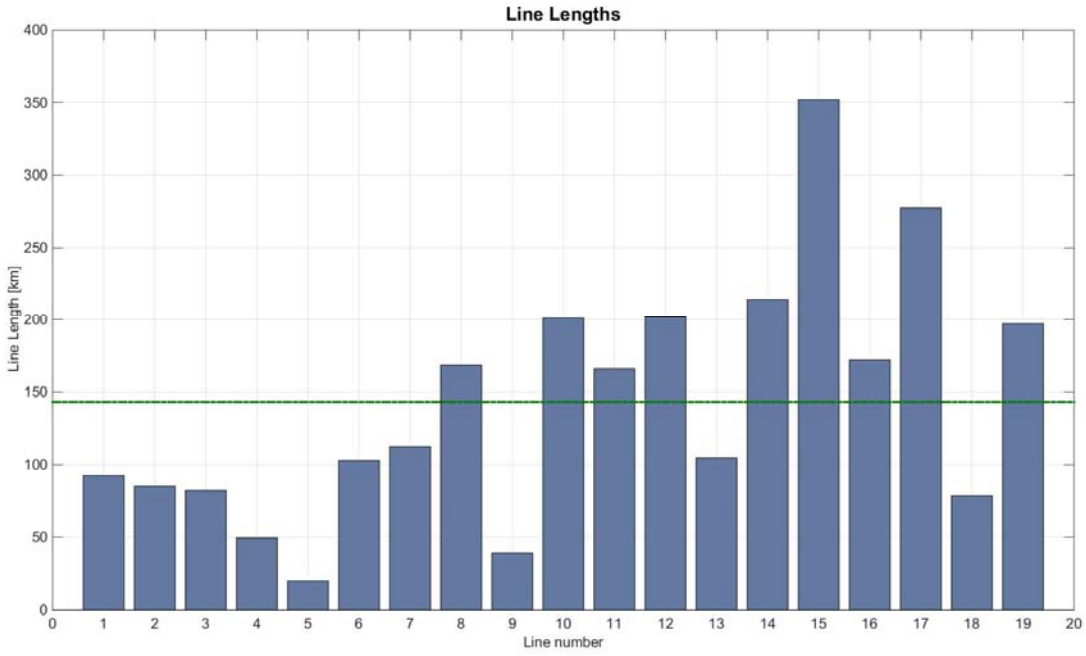

Figure 10. Line lengths of the network. Lines 5 and 9 are the shortest of the network, Line 15 that connects nodes 12 and 14, is the longest.

Classical topological analysis aims to identify the most connected nodes in the network. The degree Centrality, C_d, shows an average value of $\langle C_d \rangle = 0.1397$ for the network (Figure 11); this value means that the majority of nodes is connected to the other nodes with exactly two links. The power grid comprises few nodes with more than two links; among them, the only node that is most connected is node 11, with 4 links. The only two nodes with one link, node 16 and 17, are those connecting the Finnish and the Swedish grids.

The topological Betweenness Centrality (BC), obtained from Eq. (3.3), when g = 1, measures the importance of a node in terms of presence of the shortest paths connecting every couple of nodes in the network. One can expect that the more a node is connected, the higher will be the probability for the node to be passed through by many paths and therefore, also by many shortest paths. Figure 12 shows that node 11 has the highest betweenness centrality, followed by node 10 and node 5, as expected.

The Degree and Betweenness Centrality measures provide a first picture of the network and of its underpinning structure in terms of nodes and connections. In order to understand the physical behavior of the system we also need to consider how it functions when traversed by GICs.

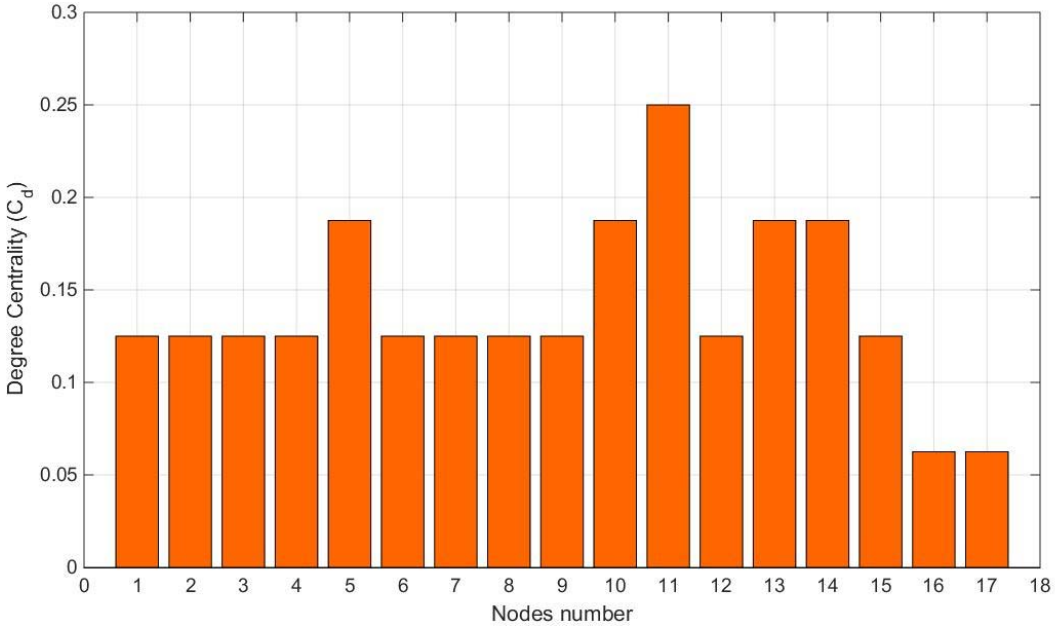

Figure 11. Degree Centrality (C_d) for the power network.

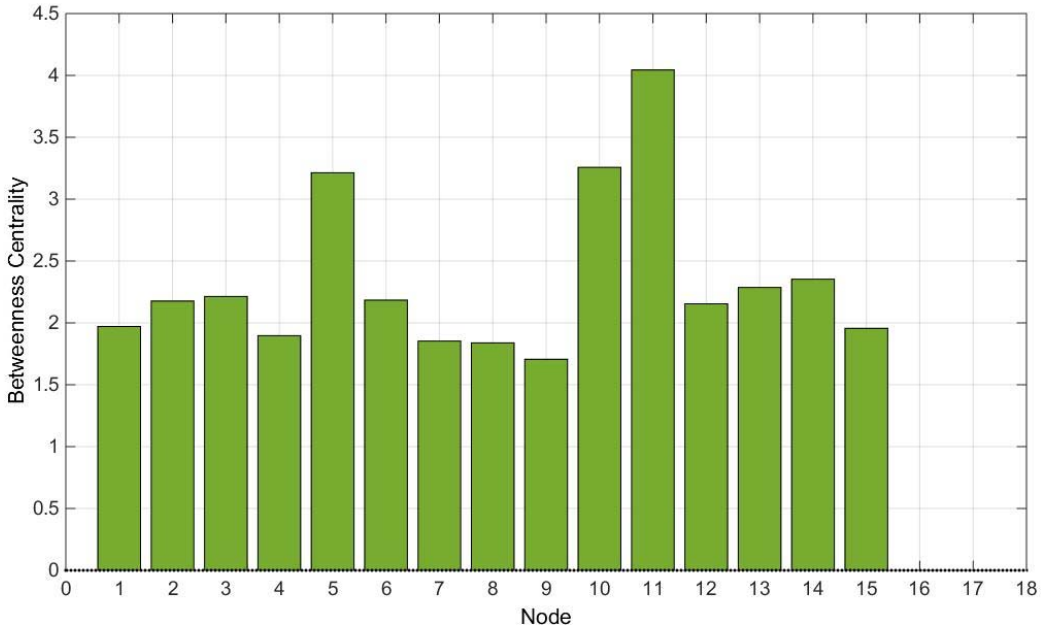

Figure 12. Betweenness Centrality (BC) for the power network.

4.1.1 Calculation of GICs: uniform electric field

In order to validate the implementation of the models, a set of baseline GICs calculations were performed assuming a uniform electric field **E** = 1V/km oriented northward and eastward and using the formula proposed by Lehtinen and Pirjola (1985) and introduced in Section 2.6:

$$\mathbf{I}^{\mathbf{e}} = \left(\mathbf{U} + \mathbf{Y}^{\mathbf{n}}\mathbf{Z}^{\mathbf{e}}\right)^{-1}\mathbf{J}^{\mathbf{e}} \tag{2.2}$$

Tables III and IV show that the obtained results are in agreement with the numerical calculations proposed in Pirjola (2009). GICs flowing to (from) the Earth are defined as positive (negative). The following vulnerability analysis is carried out considering an electric field of constant value and northward direction.

Station	GIC [A]	
	Eastward E=1V/km	Northward E=1V/km
1 = Inkoo	4.10	-107.53
2 = Loviisa	58.04	-88.57
3 = Nurmijärvi	-1.11	-35.74
4 = Lieto	-25.43	-36.78
5 = Hyyinkää	0.69	-16.17
6 = Koria	27.96	-26.41
7 = Olkiluoto	-102.48	14.89
8 = Ulvila	-20.98	8.19
9 = Kangasala	-26.20	-4.04
10 = Huutokoski	79.54	-15.38
11 = Alajärvi	-18.63	15.32
12 = Alapitkä	27.81	1.65
13 = Pikkarala	52.50	36.11
14 = Petäjäskoski	36.40	84.85
15 = Pirttikoski	68.84	63.89
16 = Letsi	-105.89	29.12
17 = Messaure	-55.16	76.62

Table III Results of the baseline calculations, showing GICs at the stations of the Finnish 400-kV transmission grid.

Line Number	Station A	Station B	GIC [A]	
			Eastward E=1V/km	Northward E=1V/km
1	1 = Inkoo	4 = Lieto	-87.68	64.16
2	1 = Inkoo	5 = Hyyinkää	83.58	43.37
3	2 = Loviisa	3 = Nurmijärvi	-103.62	0.61
4	2 = Loviisa	6 = Koria	45.58	87.96
5	3 = Nurmijärvi	5 = Hyyinkää	-102.51	36.35

6	4 = Lieto	7 = Olkiluoto	-62.25	100.94
7	5 = Hyyinkää	9 = Kangasala	-19.63	95.89
8	6 = Koria	10 = Huutokoski	17.63	114.37
9	7 = Olkiluoto	8 = Ulvila	40.22	86.05
10	8 = Ulvila	11 = Alajärvi	61.20	77.86
11	9 = Kangasala	11 = Alajärvi	6.57	99.93
12	10 = Huutokoski	11 = Alajärvi	-62.58	34.66
13	10 = Huutokoski	12 = Alapitkä	0.67	95.09
14	11 = Alajärvi	13 = Pikkarala	23.83	197.14
15	12 = Alapitkä	14 = Petäjäskoski	-27.14	93.44
16	13 = Pikkarala	15 = Pirttikoski	26.48	84.41
17	13 = Pikkarala	17 = Messaure	-55.16	76.62
18	14 = Petäjäskoski	15 = Pirttikoski	42.35	-20.52
19	14 = Petäjäskoski	16 = Letsi	-105.89	29.12

Table IV GICs flowing between stations A and B (as positive from A to B) in the line of the 400-kV Finnish transmission grid.

We apply the definition of Entropic Degree (ED) introduced in Chapter 3 to the Finnish transmission network to investigate how the degree of connection of the network influences the transit of GIC flow through the system. During geomagnetic disturbances, every line of the network acts as a source of current for the system: the induced current depends on the length and on the resistance of the transmission line but also on the magnitude of the electric field and on the orientation of the field with respect to the transmission line. Different lines converging in a node, convey GICs of different magnitude. We can consider these GICs as the weight of the contribution of each transmission line. Using Eq. (3.8), we consider not only the strength of the connections in terms of the weight of the links but also the number of the connections to each node and the distribution of the strength of the connections. Figure 13 shows that the highest value of ED is associated with the most connected node (node 11), as already seen for the Degree Centrality C_d. The difference between C_d and ED is in the different values of ED for nodes with the same degree centrality C_d. For example, nodes 3 and 6 show the same C_d but a completely different ED (Figs. 11 and 13). The links towards node 6 carry a larger amount of current compared to the links conveying to node 3.

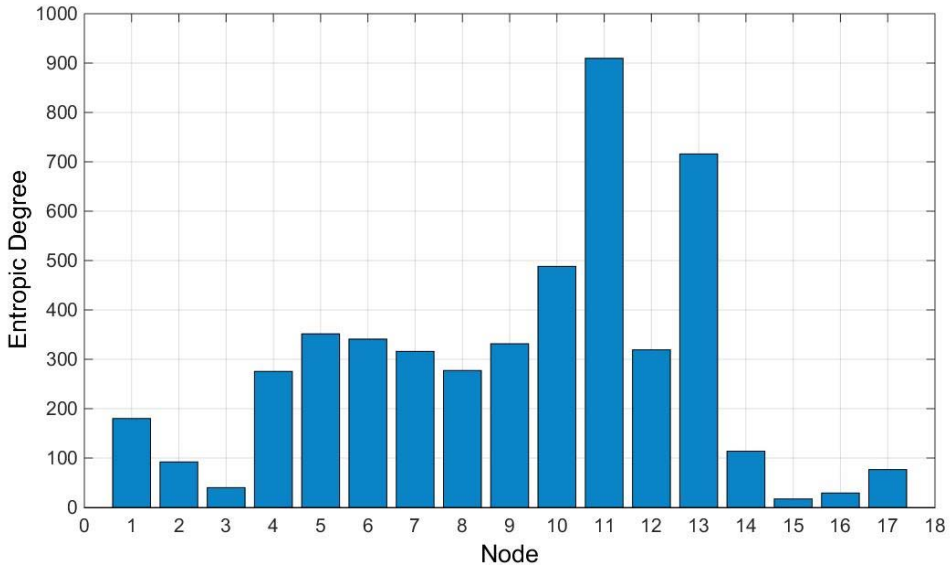

Figure 13. Entropic Degree (ED) for the 400-kV Finnish transmission grid computed using Eq. (3.8).

Upon comparing the Entropic Degree and the Degree Centrality measures, we gain more insight into the role played by the nodes in the spreading of GICs: nodes with the same number of links can give a different contribution to the diffusion of GICs The ranking of the ED values is listed in the table of Figure 14 where the three most connected nodes, in terms of ED, are nodes 11, 13 and 10.

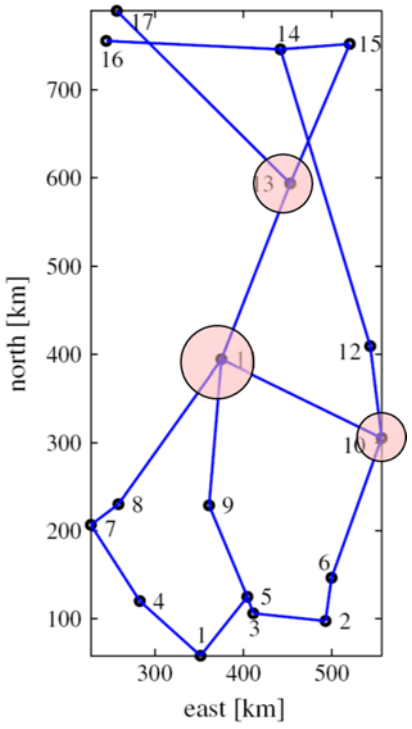

Rank	Node
1	**11**
2	**13**
3	**10**
4	**5**
5	**6**
6	**9**
7	**12**
8	**7**
9	**8**
10	**4**
11	**1**
12	**14**
13	**2**
14	**17**
15	**3**
16	**16**
17	**15**

Figure 14. Ranking of the nodes of the 400-kV Finnish power grid with respect to the Entropic Degree (ED) Centrality Measure.

In this study, the current-flow betweenness centrality (CBC) of every node *i* has been computed as the amount of current that flows through *i* averaged over all the possible paths between source and

target nodes. The current-flow betweenness centrality values give a ranking of the relevance of the nodes in current flow transmission in the network (Fig. 15).

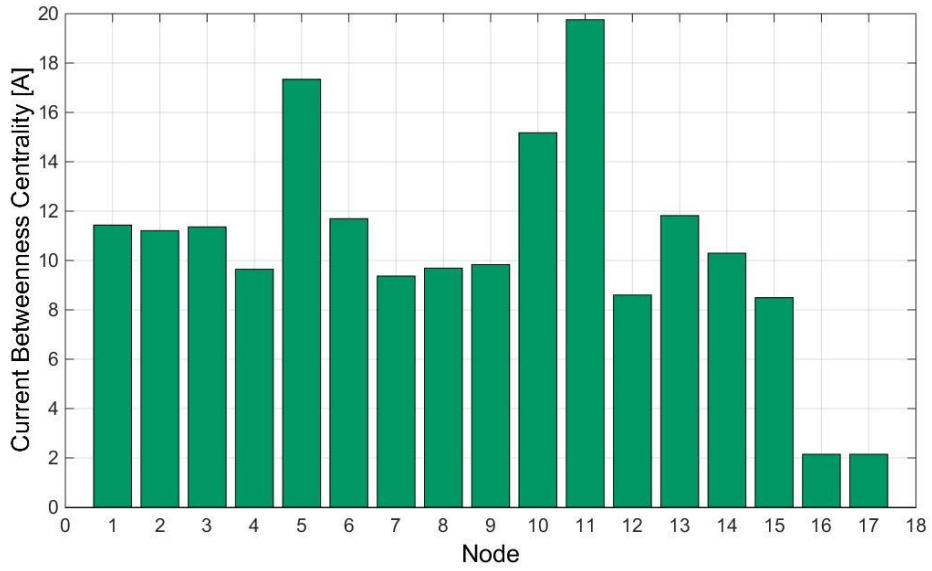

Figure 15. Current-flow betweenness centrality for the stations of the 400-kV Finnish power grid based on the topology, and on the electric behaviour of the grid.

Except for nodes 16 and 17, which are peripheral vertices, the majority of the nodes of the network appears to give nearly the same contribution to the diffusion of GICs in the network. Nodes with the highest degree (nodes 5, 10 and 13 with degree $k_5 = k_{10} = k_{13}=3$ and node 11 with $k_{11}=4$) are also nodes with the highest flow betweenness centrality. These elements mainly affect the spreading of GICs throughout the network and should be carefully monitored when planning prevention actions of GIC diffusion during solar storms.

We can also rank the nodes with respect to their CBC measure (Figure 16). Nodes 11, 5 and 10 show the highest contribution to the diffusion of GICs through the network.

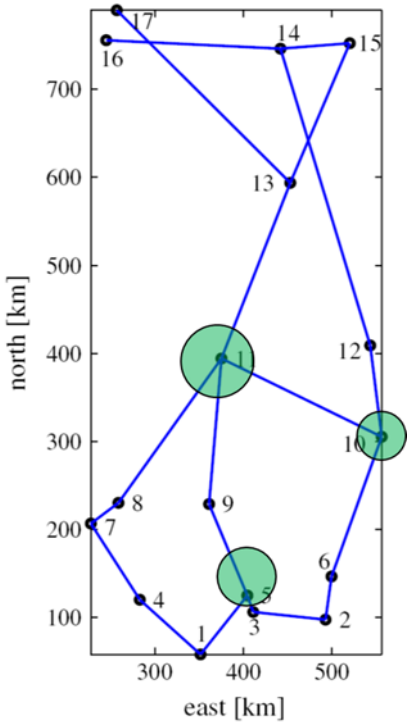

Rank	Node
1	**11**
2	**5**
3	**10**
4	**13**
5	**6**
6	**1**
7	**3**
8	**2**
9	**14**
10	**9**
11	**8**
12	**7**
13	**4**
14	**12**
15	**15**
16	**16**
17	**17**

Figure 16. Ranking of the nodes of the 400-kV Finnish power grid with respect to Current-flow Betweenness Centrality (CBC) measure.

4.1.2 Calculation of GICs: uniform electric field with varying angles

The uniform field scenarios are now assumed to vary their direction. The uniform electric field **E** = 1V/km is considered at different orientation angles, starting with the direction from south to north (where north is at zero degree), increments of 15 degrees are progressively added up to 165 degree. Electric fields of equal magnitude separated by 180 degrees give rise to the same GICs intensity, except that the sign is reversed. For each station (Figure 17) and for each line (Figure 18), GICs at different angles are represented with different colors, starting from 0 degree (in blue) passing through 90 degree (east direction, in green) to 165 degree (in red). The sign of the currents refers to the direction of the flow at the stations (Figure 17): GICs entering a node have negative values while GICs exiting a node have positive values.

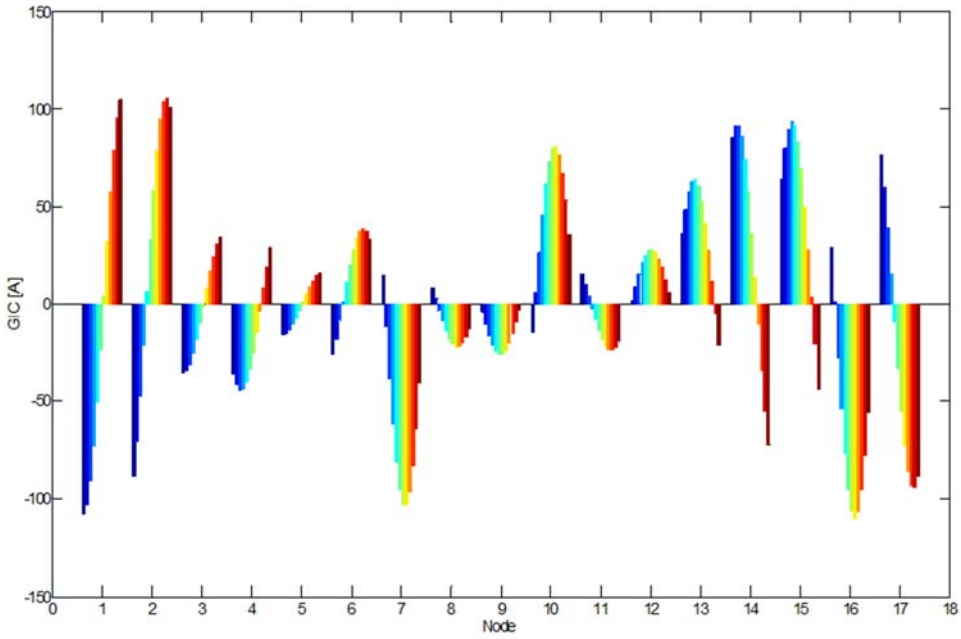

Figure 17. Representation of GICs computed for the stations of the 400 kV Finnish power grid. For each station, the different colors represent a different orientation angle of the geoelectric field **E**.

Figure 18 shows the magnitude of GICs flowing through the transmission lines. As before, each color represents a different angle between the orientations of the electric field. The sign refers to the orientation of the flow: positive values suggest that GICs flow from station A towards station B (as listed in Table II), negative values indicate that GICs flow the opposite way, from station B to station A.

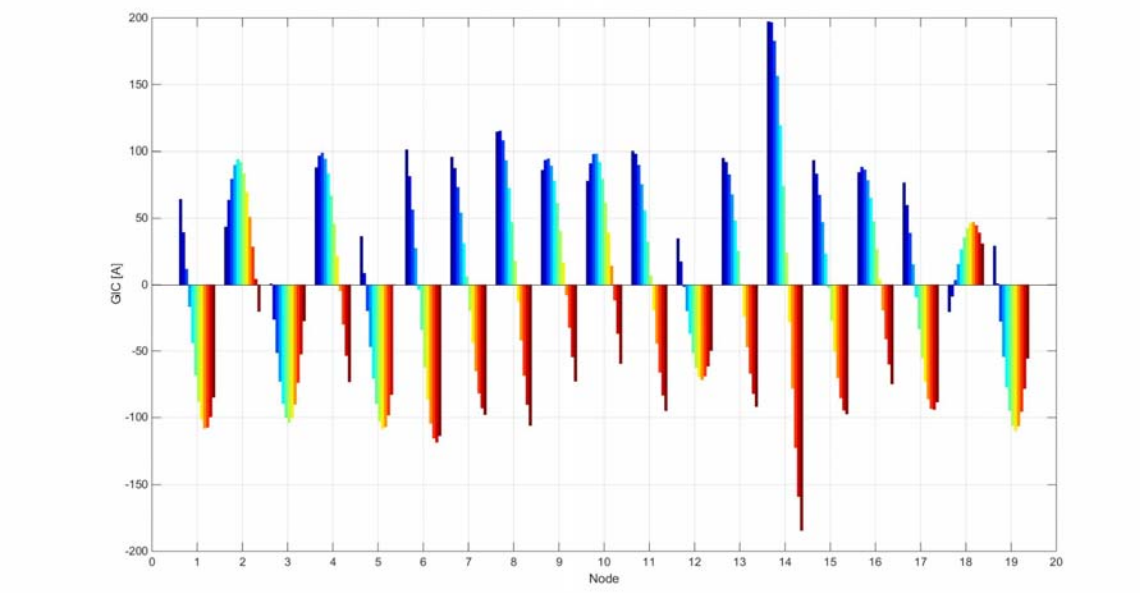

Figure 18. Representation of GICs computed for each transmission line of the 400 kV Finnish power grid. For each line, the different colors represent a different orientation angle of the geoelectric field **E**.

The ED and the CBC measures have been investigated for each different angle (Figs. 19 and 20). The Entropic Degree centrality measure represents the behavior of each node along with the variation of the orientation between the electric field and the orientation of the lines. In Fig. 19, every box

represents the entropic degree value of the system computed for a specific angle, starting from the first box in which the electric field is directed northward, (0 degree, in blue) and increasing, in each box, the orientation angle by 15 degrees until 165 degrees (dark red).

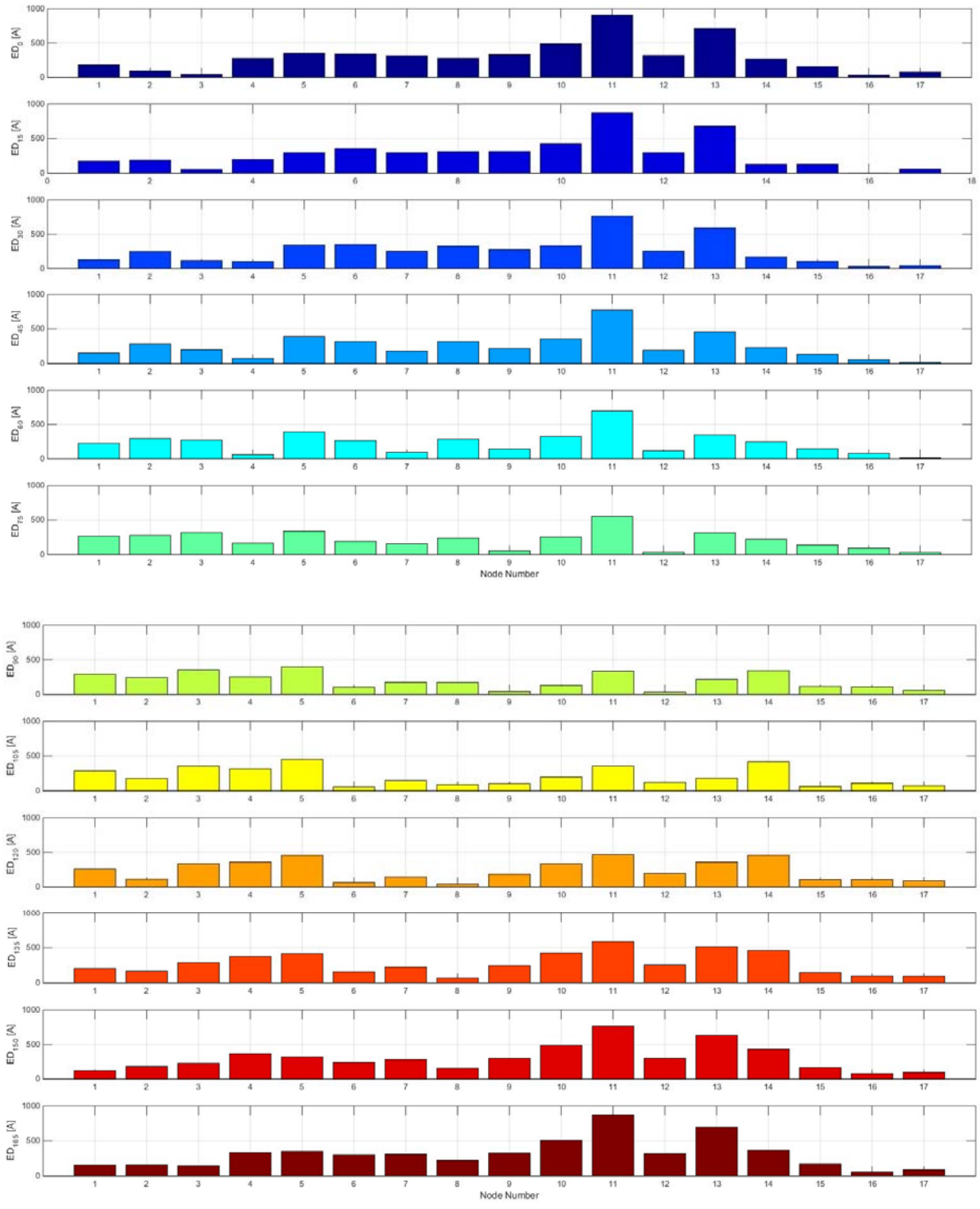

Figure 19. The Entropic Degree (ED) centrality measure is represented for each angle, starting from 0° (bar graph in the first box from the top) and continuing with an increase of 15° for each successive bar graph.

Figure 19 shows that, despite the variation of the angle between the electric field and the transmission lines, the ranking of the nodes given by the ED centrality measure does not change drastically: on average, nodes 11 and 13 maintain the highest values of ED, as shown in Table V.

ED		Orientation Angle (degree)											
		0	15	30	45	60	75	90	105	120	135	150	165
Ranking Order	1	**11**	**11**	**11**	**11**	**11**	**11**	**5**	**5**	**11**	**11**	**11**	**11**
	2	**13**	**13**	**13**	**13**	**5**	**5**	**3**	**14**	**14**	**13**	**13**	**13**
	3	**10**	**10**	**6**	**5**	**13**	**3**	**14**	**11**	**5**	**14**	**10**	**10**
	4	**5**	**6**	**5**	**10**	**10**	**13**	**11**	**3**	**4**	**10**	**14**	**14**
	5	**6**	**9**	**10**	**6**	**2**	**2**	**1**	**4**	**13**	**5**	**4**	**5**
	6	**9**	**8**	**8**	**8**	**8**	**1**	**4**	**1**	**3**	**4**	**5**	**4**
	7	**12**	**12**	**9**	**2**	**3**	**10**	**2**	**10**	**10**	**3**	**12**	**9**
	8	**7**	**5**	**12**	**14**	**6**	**8**	**13**	**13**	**1**	**12**	**9**	**12**
	9	**8**	**7**	**7**	**9**	**14**	**14**	**7**	**2**	**12**	**9**	**7**	**7**
	0	**4**	**4**	**2**	**3**	**1**	**6**	**8**	**7**	**9**	**7**	**6**	**6**
	11	**14**	**2**	**14**	**12**	**15**	**4**	**10**	**12**	**7**	**1**	**3**	**8**
	12	**1**	**1**	**1**	**7**	**9**	**7**	**15**	**16**	**2**	**2**	**2**	**15**
	13	**15**	**15**	**3**	**1**	**12**	**15**	**16**	**9**	**16**	**6**	**15**	**2**
	14	**2**	**14**	**15**	**15**	**7**	**16**	**6**	**8**	**15**	**15**	**8**	**1**
	15	**17**	**17**	**4**	**4**	**16**	**9**	**17**	**17**	**17**	**16**	**1**	**3**
	16	**3**	**3**	**17**	**16**	**4**	**12**	**9**	**15**	**6**	**17**	**17**	**17**
	17	**16**	**16**	**16**	**17**	**17**	**17**	**12**	**6**	**8**	**8**	**16**	**16**

Table V. Ranking of the nodes of the system according to the importance given by the entropic degree centrality measure (ED).

However, the entropic degree values decrease in magnitude with the increase of the orientation angle (Fig. 20). For example, we can fix the attention on node 11 and follow the trend of the colored bar along the field orientation angle direction. Starting from the dark blue bar and following the shades of blue along node 11, we can see a decrease in the ED measure until the green bar, where ED for node 11 is at its minimum. Then, continuing with increasing angles, the ED value increases again (following shades from yellow to dark red).

The ranking of the nodes with respect to the ED centrality measure reproduced in Table V shows that, in general, the importance (ranking) of the nodes does not change with the variation of the orientation angle. However, there is a change when the orientation angle is 90 and 105°, which corresponds to the electric field being oriented eastward. In our definition, ED measures the connectivity of the network in term of GICs that traverse it. A major contribution to the spreading of GICs is given when the electric field is “aligned” with the orientation of the transmission lines. Nodes 11 and 13 in the 400-kV transmission power grid connect lines whose principal components are directed mainly northward. Their contribution is possible when the electric field is oriented eastward: in this latter case, lines that have a major eastward component give the highest contribution to the spreading of GICs and are connected by nodes 5 and 14, which, in this case, become critical with respect to GICs.

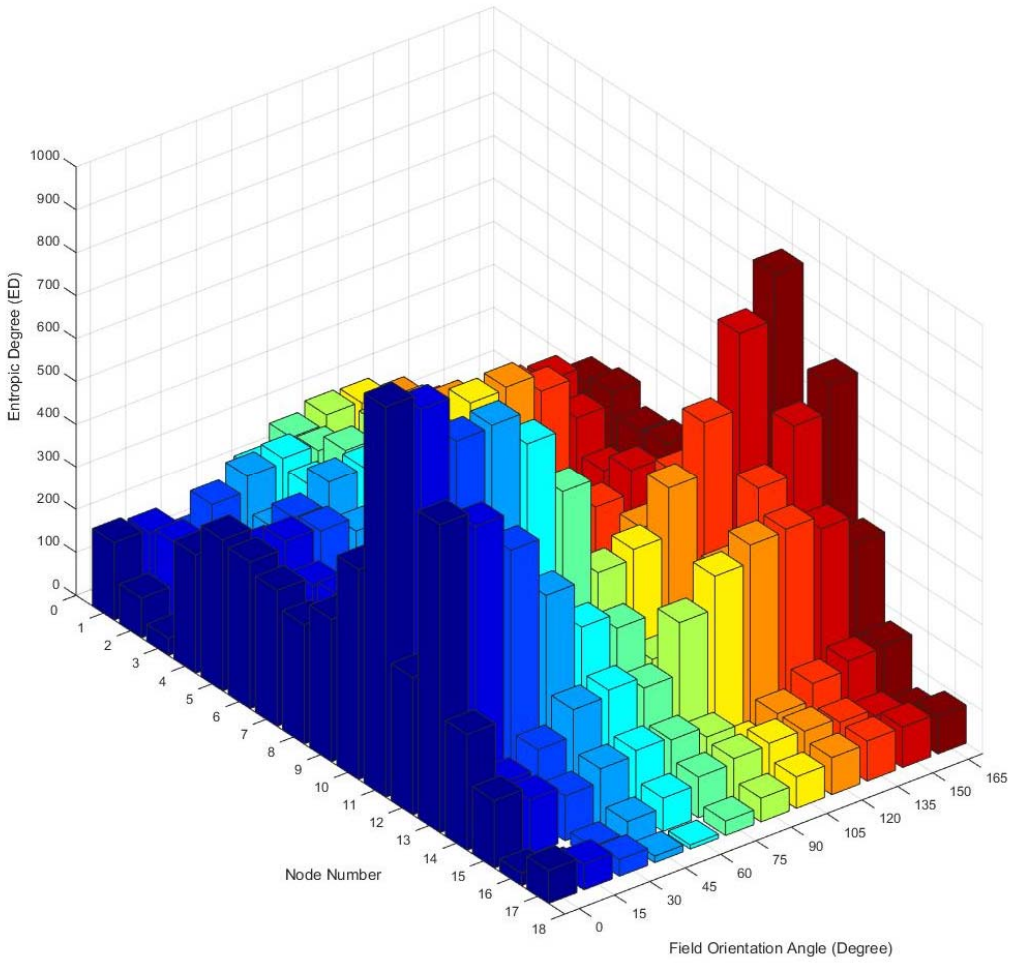

Figure 20. Three-dimensional representation of the Entropic Degree (ED). The centrality measure is shown for all the stations for each angle, starting from 0 degrees (blue bar on the left) and continuing with an increase of 15° for each successive bar to 165° (last red bar on the right).

Similarly, the Current-flow Betweenness computed for the different angle orientations considered, is represented in Fig. 21, and the ranking of nodes with respect to CBC is listed in Table VI. For CBC, the different orientations of the electric field do not affect the ranking for node 11. In this case, those nodes which are traversed more by the flow are more important. These are the nodes with the highest connection degree: nodes 11, with 4 connections and nodes 5, 13 and 10, with three connections each.

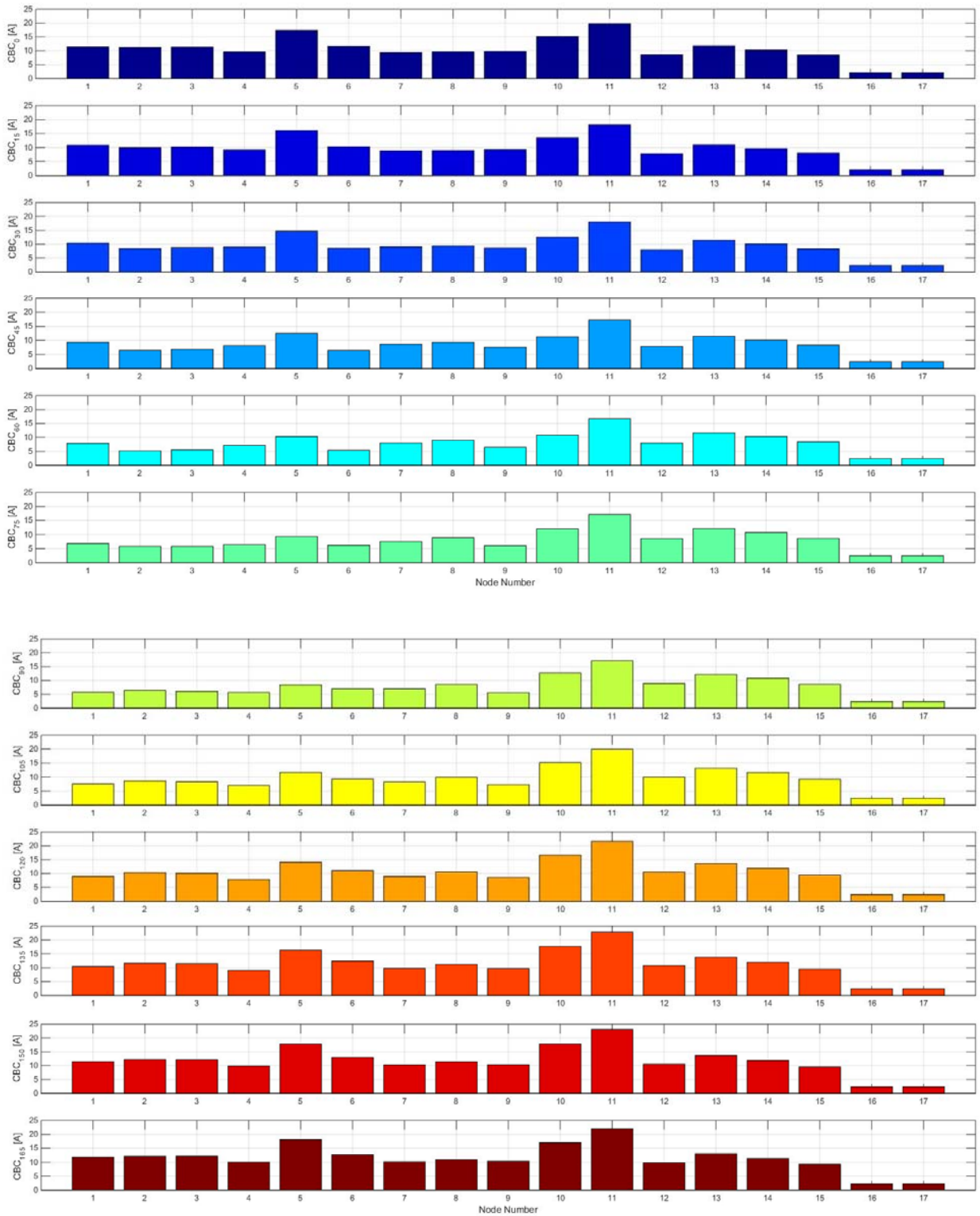

Figure 21. Bar-Plots of the Current-flow Betweenness Centrality (CBC). Each color represent an angle, starting from 0° (top plot, blue), and continuing with 15° increments until 165° (dark red, bottom plot).

CBC		Orientation Angle (degrees)											
		0	15	0	45	60	75	90	105	120	135	150	165
Ranking order	1	**11**	**11**	**11**	**11**	**11**	**11**	**11**	**11**	**11**	**11**	**11**	**11**
	2	**5**	**5**	**5**	**5**	**13**	**13**	**10**	**10**	**10**	**10**	**10**	**5**
	3	**10**	**10**	**10**	**13**	**10**	**10**	**13**	**13**	**5**	**5**	**5**	**10**
	4	**13**	**13**	**13**	**10**	**14**	**14**	**14**	**5**	**13**	**13**	**13**	**13**
	5	**6**	**1**	**1**	**14**	**5**	**5**	**12**	**14**	**14**	**6**	**6**	**6**
	6	**1**	**6**	**14**	**1**	**8**	**8**	**15**	**12**	**6**	**14**	**2**	**3**
	7	**3**	**3**	**8**	**8**	**15**	**15**	**8**	**8**	**8**	**2**	**3**	**2**
	8	**2**	**2**	**7**	**7**	**7**	**12**	**5**	**6**	**12**	**3**	**14**	**1**
	9	**14**	**14**	**4**	**15**	**12**	**7**	**6**	**15**	**2**	**8**	**1**	**14**
	10	**9**	**9**	**3**	**4**	**1**	**1**	**7**	**2**	**3**	**12**	**8**	**8**
	11	**8**	**4**	**9**	**12**	**4**	**4**	**2**	**3**	**15**	**1**	**12**	**9**
	12	**4**	**8**	**6**	**9**	**9**	**6**	**3**	**7**	**1**	**7**	**9**	**7**
	13	**7**	**7**	**2**	**3**	**3**	**9**	**1**	**1**	**7**	**9**	**7**	**4**
	14	**12**	**15**	**15**	**2**	**6**	**2**	**4**	**9**	**9**	**15**	**4**	**12**
	15	**15**	**12**	**12**	**6**	**2**	**3**	**9**	**4**	**4**	**4**	**15**	**15**
	16	**17**	**17**	**17**	**17**	**17**	**17**	**16**	**16**	**17**	**16**	**17**	**17**
	17	**16**	**16**	**16**	**16**	**16**	**16**	**17**	**17**	**16**	**17**	**16**	**16**

Table VI. Ranking of the nodes of the system according to the importance given by the current-flow betweenness centrality measure (CBC).

4.2 Power Flow and GICs

Work is in progress on adding GICs in a power grid system under load flow. A scoping study was carried out, the results of which are described in the following section.

No data on bus loads or generators capacity are publicly available for the model of the 400kV-transmission power grid proposed as a benchmark case. As a consequence, we inferred the values for the requested and supplied power from statistics available at the websites of the Finnish Energy Authority (2014), the Finnish transmission power grid operator (Fingrid Oyj, 2014) and the European Network of Transmission System Operators for Electricity (ENTSOE, 2014). This data are summarized in Tables VII e VIII.

The percentage of system load was assigned to every single node on the basis of the statistics on the power consumption of each area served by the stations listed in the first column of Table VII. Following the example proposed in Grigg (1999), the reactive part of the loads (forth column) was interpolated from the reliability test system RTS96.

Station	Bus load	Load	
	% of System Load	[MW]	[MVAr]*
1 = Inkoo	10.8	458	93
2 = Loviisa	5.4	229	47
3 = Nurmijärvi	9.5	403	82

4 = Lieto	5.6	237	49
5 = Hyyinkää	4.5	191	39
6 = Koria	3.7	157	32
8 = Ulvila	8.2	348	71
9 = Kangasala	6.1	259	53
10 = Huutokoski	4.2	178	36
11 = Alajärvi	6.3	267	55
12 = Alapitkä	3.5	148	30
13 = Pikkarala	5.7	242	49
14 = Petäjäskoski	11	466	95
15 = Pirttikoski	11.1	471	96
16 = Letsi	2.1	89	18
17 = Messaure	2.3	97	20
Total	100	4240	865

Table VII. Table of real power and reactive power demand for the system loads (* MVAr is the unit for reactive power).

Data on generating units (Table VIII) show that more than half of the supplied power is produced by the nuclear power plants located at Loviisa and Olkiluoto. This latter is also assumed as the slack node of the transmission grid.

Station	Unit Size [MW]	Unit type
1 = Inkoo	690	Coal
2 = Loviisa	1032	Nuclear/Fossil fuel
4 = Lieto	330	Coal
6 = Koria	160.5	Fossil fuel/Biomass
7 = Olkiluoto	1860.5	Nuclear/Fossil
8 = Ulvila	285	Biomass/Coal
9 = Kangasala	333	Fossil fuel/Coal
10 = Huutokoski	180	Fossil fuel/Biomass
13 = Pikkarala	195	Fossil fuel/Biomass
Total	5066	

Table VIII. Table of the generating unit type and capacity for the system.

Once GICs have been calculated for every node, their effect needs to be inserted into the transmission power grid model. As introduced in Section 2.4, GICs can induce saturation in transformers and, as a main consequence, cause reactive power losses (Kappenman, 2010; Overbye et al., 2012). If the system cannot supply the increase in reactive power demand, it can eventually collapses.

Following the observations of Albertson et al. (1973) and Walling and Kahn (1991), we adopt the assumption that each transformer's reactive power losses Q_{loss} vary linearly with GICs and with the voltage of the bus:

$$Q_{loss} = V_{kV} k I_{gic} \quad (4.1)$$

In Equation (4.1) V_{kV} is the station voltage, expressed in kV, I_{gic} is the current induced in the transformer, expressed in Ampère, and k is a transformer specific constant. In principle, the value k for each transformer should be known. In this study, we consider the constant k to have, for all the transformers, a value equal to 2.8, as suggested in the literature (Albertson et al., 1981).

GICs computed for different scenarios have been included in the AC power flow for the 400kv Finnish transmission power grid, as shown in Fig. 22.

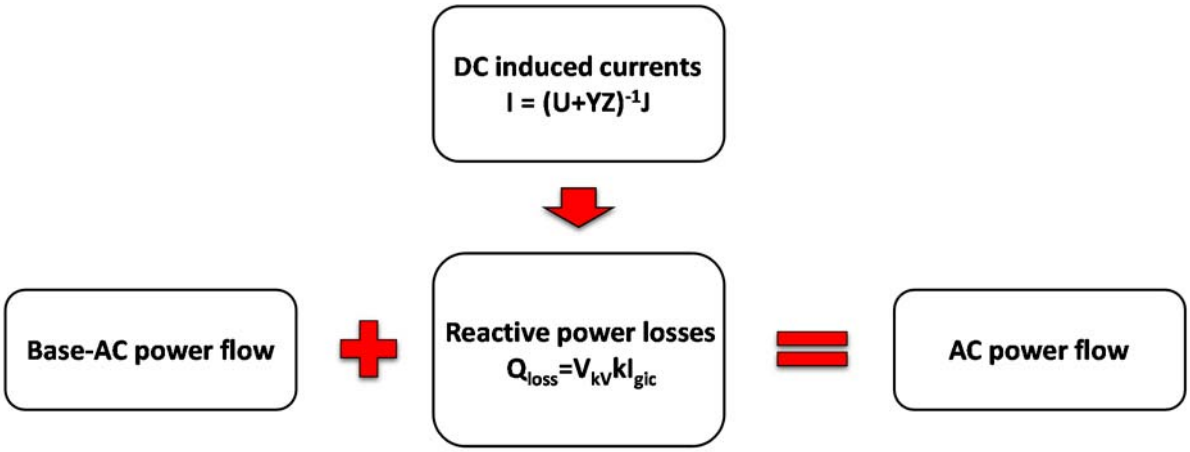

Figure 22. Outline of the method employed to evaluate the load flow in the 400kV transmission grid in the presence of GICs.

For our scoping study we considered four scenarios. In each of them we increased the magnitude of the electric field, which assumes the peak values computed by Pulkkinnen (2012): $|\mathbf{E}|$=1V, 2V, 5V and 20V. For each of these electric field magnitudes and for each orientation angle, the resulting AC power flow has been calculated using MATPOWER (2011). The collapse of the system was signaled by the non-convergence of the power flow calculation. Results are summarized in Table IX.

	0	15	30	45	60	75	90	105	120	135	150	165
$\|\mathbf{E}\|$=1V												
$\|\mathbf{E}\|$=2V												
$\|\mathbf{E}\|$=5V												
$\|\mathbf{E}\|$=20V												

Table IX. Schematic representation of the convergence of the power flow algorithm for the 400-kV power transmission power grid. Convergence is represented by green boxes; red boxes represent collapse of the system.

The first results of this study seem to indicate that the system can resist GICs induced from high intensity electric fields. Moreover, the network seems more prone to collapse when the electric field has a northward direction, as shown by the red boxes in Table IX.

4.3 Discussion

In this study, complex network theory has been used to investigate the vulnerability of the power network to space weather impact. The ranking of nodes with respect to ED and CBC centrality measures identifies the most important nodes of the network with respect to GICs: nodes with the highest number of links contribute the most in the diffusion of GICs through the network. Since we want to avoid GICs to flow throughout the system, these are the critical nodes to monitor when considering mitigation measures, in order to avoid effects leading to possible blackouts.

The analysis of the behavior of the system affected by an electric field with different orientation shows little variation of the importance of nodes with varying angles. However, there are changes in the ranking of the nodes, as shown in Tables VII and VIII. The electric field integrated along the transmission lines acts as a voltage generator (Eq. (2.7)) for the network and, since the geoelectric field is rotational, the integral depends on the path between nodes. In particular, since the geovoltage is the result of an inner product, it depends on the electric field and on the projection of the length of the transmission line alongside the direction of the electric field. We kept the geoelectric field magnitude uniform so the varying contribution to the geovoltage is given by the projection of the "global length" of the network. If one focuses on the two principal directions, north and east, one realizes that the network expands more in the northward than the eastward direction, thus a strong geoelectric field directed northward will have a more pronounced impact on the network.

Table IX confirms this finding. It represents the risk for the power grid in AC load-flow regime to collapse due to extreme space weather. Non-convergence for the system occurs when the magnitude of the geoelectric field is high and directed northward. In our study, the dependence of the orientations of power lines with respect to the geoelectric field results more pronounced than in the study of in Pirjola (2002).

Further work is underway to analyze the vulnerability of power grids to space weather impact in more detail, including the refinement of assumptions and models to arrive at a unified assessment of the associated risk at EU level.

5. Conclusions

During geomagnetic storms, high voltage transmission grids are particularly exposed to damage: induced geomagnetic currents (GICs) can damage transformer equipment and cause voltage instability, possibly causing power systems to collapse.

Power systems are large-networked engineered systems, whose complexity and vulnerability to hazards and failures can be investigated by means of complex network theory. By representing stations with nodes and transmission lines with links between nodes, complex systems can be described by models that are abstract enough for handling the computational burden and that are nevertheless representative of the physical behavior of the system.

In the proposed study, we investigated the vulnerability of power grids to space weather. The assessment was performed by means of vulnerability indicators applied to a benchmark case study. The aim of the study was to understand how the structural and physical characteristics of the network influence and drive the spreading of GICs during a geomagnetic storm, and to identify which components in the network are more involved. This is the basis for understanding the behavior of the system under a “geomagnetic” stress and eventually, identifying where and how to best implement mitigation strategies.

Work is in progress to further validate and expand our approach with the aim to eventually carry out a risk assessment of the power grid at EU level. This requires an assessment of the likelihood for a system to experience a strong geomagnetic storm and of the potential consequences. A part of this study has already been implemented into the Joint Research Centre’s Global Resilience and Risk Assessment Platform (GRRASP) which we will at a later stage use to model ripple effects due to space weather induced power grid failure via interdependencies with other critical infrastructures.

References

Albert, R., Albert, I., Nakarado, G.L., Structural vulnerability of the North American power grid, *Phys. Rev E* 69, 025103 (R), 2004.

Albert, R., Jeong, H. and Barabási, A.-L., Error and attack tolerance of complex networks, *Nature*, Vol. 406, 378-382, 2000.

Albertson V.D., Kappenman J.G, Mohan N. and Skarbakka G.A., Load-flow studies in the presence of geomagnetically induced currents, *IEEE Transactions on Power Apparatus and Systems*, PAS 100, 2, 594-607, 1981.

Albertson V.D., Thorson J.M., Clayton R.E., and Tripathy S.C., Solar-induced-currents in power systems: cause and effects, *IEEE Transactions on Power Apparatus and Systems*, PAS 92, 2, 471-477, 1973.

Belov A.V., Gaidash S.P., Eroschenko E. A., Lobkov V.L., Pirjola r., Trichtchenko L., Effects of strong geomagnetic storms on northern railways in Russia, *Proceedings of 7th International Symposium and Exhibition on Electromagnetic Compatibility and Electromagnetic Ecology (IEEE EMC)*, Sankt Petersburg, 280–282, 2007.

BGS, http://www.geomag.bgs.ac.uk/documents/BGS_Carrington_poster.pdf. British Geological Survey. Accessed on 21st October 2014.

Boccaletti, S., Latora, V., Moreno, Y., Chavez, M. and Hwang, D.-U., Complex Networks: structure and Dynamics, *Physics Reports*, 424, 175-308, 2006.

Bompard E., Napoli R., Xue F., Analysis of structural vulnerabilities in power transmission grids, *International Journal of Critical Infrastructure Protection*, 2, 5-12, 2009.

Boteler, D.H., Assessment of geomagnetic hazard to power systems in Canada, *Natural Hazards*, 23, 101-120, 2001.

Boteler D.H., Pirjola R., Nevanlinna, The effects of geomagnetic disturbances on electrical systems at the Earth's surface, *Advances in Space Research*, Vol. 22, 17-27, 1998.

Boteler D.H., Distributed-source transmission line theory for electromagnetic induction studies, *Supplement of the Proceedings of the 12th International Zurich Symposium and Technical Exhibition on Electromagnetic Compatibility*, Zürich, Switzerland, February 18-20, 401–408, 1997.

Bouchon S., The vulnerability of interdependent critical infrastructures systems: epistemological and conceptual state-of-the-art, *EUR 22205 EN*, 2006.

Brancucci Martinez-Anido C., Bolado R., De Vries L., Fulli G., Vandenbergh M. and Masera M., European power grid reliability indicators, what do they really tell?, *Electric Power System Research*, 90, 79-84, 2012.

Cadini, F., Zio, E. and Petrescu, C.A., Using Centrality Measures to Rank the Importance of the Components of a complex Network Infrastructure, in *Critical Information Infrastructure Security*, Proceedings of the 3rd International Workshop on Critical Information Infrastructures Security, CRITIS 2008, Rome, Italy, October 13-15, 2008, 155-167, 2009.

Crucitti, P., Latora, V. and Porta, S., Centrality in networks of urban streets, *Chaos*, 16, 015113, 2006.

Dong B., Wang Z., Boteler D. and Pirjola R., Review of Earth conductivity structure modeling for calculating geo-electric Fields, *Power and Energy Society General Meeting (PES)*, IEEE Proceeding of conference held in Vancouver, Canada, 21-25 July, 2013.

Dueňas-Osorio, L., Craig, I.J., Goodno, J.B. and Bostrom, A., Interdependent Response of Networked Systems, *J. Infrastruct. Syst.*, vol. 13, Issue 3, 185-194, 2007.

Eroshenko E. A., Belov A. V., Boteler D., Gaidash S. P., Lobkov S. L., Pirjola R., and L. Trichtchenko, "Effects of strong geomagnetic storms on Northern railways in Russia," *Advances in Space Research*, Vol. 46, 1102-1110, 2010.

Eusgeld, I., Koger, W., Sansavini, G., Schapfer, M., Zio, E., "The role of network theory and object-oriented modeling within a framework for the vulnerability analysis of critical infrastructures", *Reliability Engineering & Systems Safety*, 94(5), 954–963, 2009.

Everett, M.G., Borgatti, S.P., The centrality of groups and classes, *Journal of Mathematical Sociology*, Vol. 23, N. 3, pp. 181-201, 1999.

FEN, Geomagnetically induced currents in the Swiss transmission network - A technical study commissioned by the Swiss Federal Office of Energy and Swissgrid, Research Centre for Energy Networks – ETH Zurich, 2013.

Fingrid Oyj, http://www.fingrid.fi/en. Accessed on 5th November 2014.

Finnish Energy Authority, http://www.energiavirasto.fi/en/web/energy-authority. Accessed on 5th November 2014.

Ford, L. and Fulkerson, D., *Flows in Networks*, Princeton University Press, Princeton, NJ, 1962.

Freeman, L.C., Borgatti, S.P., and White, D.R., Centrality in valued graphs: A measure of betweenness based on network flow, *Social Networks* 13(2): 141-154, 1991.

Freeman, L. C., Centrality in social networks conceptual clarification, *Social Networks*, 1(3), 215-239, 1979.

Grigg, C., and Wong, P., The IEEE Reliability Test Sytem 1996, *IEEE Transaction on Power Systems*, 14, 101-1020, 1999.

GSC, http://www.nrcan.gc.ca/earth-sciences/. Accessed on 21st October, 2014.

Gummow, R.A., GIC effects on pipeline corrosion and corrosion control systems, *Journal of atmospheric and Solar-Terrestrial Physics*, 64, 1755-1764, 2002.

Haimes, Y.Y., On the definition of vulnerability in measuring risk to infrastructures, *Risk Analysis*, 26, 2, 293-296, 2006.

Hines, P. and Blumsack, S., A centrality measure for electrical networks, *Proceedings of the 41st Hawaii International Conference on system Science*, 2008.

Horton, R., Boteler, D., Overbye, T.J., Pirjola, R. and Dugan, R.C., A test case for the calculation of geomagnetically induced currents, *IEEE Transactions on power delivery*, Vol. 27, No. 4, 2012.

IEEE, Geomagnetic disturbance effects on power systems. Working Group on Geomagnetic Disturbances, *IEEE Transactions on Power Delivery*, 8(3), 1993.

INGV, Istituto Nazionale di Geofisica e Vulcanologia: http://roma2.rm.ingv.it. Accessed on 21st October 2014.

InterMagnet International Consortium, www.intermagnet.org. Accessed on 5th November 2014.

JASON, Impact of severe space weather on the electric grid, *JSR-11-320*, The MITRE Corporation, 2011.

Johansson, J., Hassel, H. and Zio, E., Reliability and vulnerability analysis of critical infrastructures: comparing two approaches in the context of power systems, *Reliability Engineering and System Safety*, 120, 27-38, 2012.

Johansson, J., Hassel, H and Cedergen, A., Vulnerability analysis of interdependent critical infrastructures: case study of the Swedish railway systems, *International Journal of Critical Infrastructures*, Vol. 7, No. 4, 289-316, 2011.

Johansson ,J. and Hassel, H., An approach for modelling interdependent infrastructures in the context of vulnerability analysi, *Reliability Engineering and System Safety*, 95, 1335-1344, 2010.

Johansson, J., and Jonsson, H., A model for vulnerability analysis of interdependent infrastructure networks, *Safety, Reliability and Risk Analysis: Theory, Methods and Applications* – Martorell et al. (eds), 2009.

Kappenman, J., Geomagnetic storms and their impacts on the US power grid, *Meta – R- 319 Report*, 2010.

Kappenman, J., Geomagnetic storms and their impact on power systems, *IEEE Power Engineering review*, 1996.

Koen, J, and Gaunt, T., Geomagnetically indced currents in the southern African electricity transmission network, *Proceedings of the IEEE Power Tech Conference*, Bologna, June 23-26, 2003.

Krausmann, E., Andersson, E., Murtagh, W. and Mitchison, N., Space weather and power grids: findings and outlook, *EUR 26370*, ISBN 978-92-79-34812-9, 2013.

Kröger, W., Zio, E., *Vulnerable systems*, Springer-Verlag London Limited 2011.

Latora, V., and Marchiori, M., A Measure of Centrality Based on the Network Efficiency, *New Journal of Physics*, 9, 188, 2007.

Latora, V. and Marchoiri, M., Vulnerability and protection of infrastructure networks, *Physical Review E* 71, 015103 (1-4), 2005.

Latora, V. and Marchiori, M., Efficient Behavior of Small-World Networks, *Physical Review Letters*, vol. 87, 19, pp. 198701(1-4), 2001.

Lehtinen, M., and Pirjola, R., Currents produced in earthed conductor networks by geomagnetically-induced electric fields, *Annales Geophysicae*, 3, 479–484, 1985.

MATPOWER: Zimmerman R.D., Murillo-Sànchez and Thomas R.J., MATPOWER: steady-state operations, planning and analysis tools for power system research and education, *IEEE Transactions on Power Systems*, Vol. 26, No. 1, 12-19, 2011.

Molinski, T., Why utilities respect geomagnetically induced currents, *Journal of Atmospheric and solar and terrestrial Physics*, 64, 1765-1778, 2002.

Molinski, T., and Feero, W.E., Shielding grids from solar storms, *IEEE Spectrum*, 2000.

NASA, National Aeronautics and Space Administration: http://sec.gsfc.nasa.gov/popscise.jpg. Accessed on 21st October 2014.

NERC, GMDTF Interim Report: Effects of Geomagnetic disturbances on the Bulk power system, North American Electric Reliability Corporation, 2012.

Newman, M.E., A measure of betweenness centrality based on random walks, *Social Networks*, Vol. 27, No. 1, 39-54, 2005.

Ngneugueu, T., Marketos, F., Devaux, F, Bardsley, R, Xu, T., Barker, S., Baldauf, J. and Oliveira, J., Behaviour of transformers under DC/GIC excitation: phenomenon, impact on design/design evaluation process and modelling aspect in support of design, *Proceedings of CIGRE*, Paris, August 26-31, 2012.

Niemen, J., On the centrality in a graph, *Scandinavian Journal of Psychology,* 15(1), pp. 332-336, 1974.

NRC, National Research Council, Severe Space Weather Events—Understanding Societal and Economic Impacts, Workshop Report, ISBN 978-0-309-12769-1, 2008.

Overbye, T.J., Hutchins, T.R., Shetye, K., Weber, J., and Dahamn, S., Integration of geomagnetic disturbance modeling into the power flow: a methodology for large-scale system studies, *Proceedings of the North American Power Symposium*, University of Illinois, September 9-11, 2012.

Patterson, S. and Apostolakis, G., Identification of critical locations across multiple infrastructures for terrorist actions, *Reliability Engineering & System Safety*, 92(9), pp. 1183-1203, 2007.

Piccinelli, R., Methods for the vulnerability analysis of critical infrastructures, PhD thesis, Politecnico di Milano, 2013.

Pirjola, R., Geomagnetically induced currents as ground effects of space weather, 2012, available at: http://cdn.intechopen.com/pdfs-wm/33700.pdf. Accessed on 10th November, 2014.

Pirjola, R., Fundamentals about the flow of geomagnetically induced currents in a power system applicable to estimating space weather risks and designing remedies, *Journal of Atmospheric and Solar-Terrestrial Physics*, 64, 1967-1972, 2002.

Pirjola, R., Viljanen, A., Pulkkinen, A. and Amm, O., Space weather risk in power systems and pipelines, *Physics and Chemistry of the Earth*, Vol. 25, No. 4, 333-337, 2000. Lehtinen, M. and Pirjola, R., Currents produced in earthed conductor networks by geomagnetically-induced electric fields, *Annales Geophysicae*, 3, 479-484, 1985.

Pracser, E., Adam, A. and Wesztergom, W., Estimation of the electric resistivity distribution (EUROHM) in the European lithosphere in the frame of the EURISGIC WP2 project, *Acta Geodaetica et Geophysica Hungarica*, Vol. 47, No. 4, 377-387, 2012.

Ptitsyna, N. G., Kasinskii, V. V., Villoresi, G., Lyahov, N. N., Dorman, L. I., and Iucci, N., Geomagnetic effects on mid-latitude railways: A statistical study of anomalies in the operation of signaling and train control equipment on the East-Siberian Railway, *Advances in Space Research*, Vol. 42, No. 9, 1510-1514, 2008.

Pulkkinen, A., Bernabeu, E., Eichner, J., Beggan, C. and Thomson, A.W.P., Generation of 100-year geomagnetically induced current scenarios, Space Weather, 10, 2012.

Pulkkinen, A., Pirjola, R., Boteler, D., Viljanen, A., and Yegorov, I., Modelling of space weather effects on pipelines, Journal of Applied Geophysics, 48, 233-256, 2001.

Püthe, C. and Kuvshinov, A., Towards quantitative assessment of the hazard from space weather. Global 3-D modellings of the electric field induced by a realistic geomagnetic storm, *Earth Planet Space*, 65, 1017-1025, 2013.

Rodrigue, J.-P., Department of Global Studies & Geography, Hofstra University, New York, USA. http://people.hofstra.edu/geotrans/eng/ch9en/conc9en/map_probability_geomagnetic_storm.html Accessed on 22 October, 2014.

Rosas-Casals, M. and Solé, R., Analysis of major failures in Europe's power grid, *Electrical Power and Energy Systems*, 33, 805-808, 2011.

Rosas-Casals M., Valverde, S. and Solé, R., Topological vulnerability of the European power grid under errors and attacks, *Int. J. Bifurcation and Chaos*, Vol.17, No.07, 2007.

Rosato, V., Bologna, S. and Tiriticco, F., Topological properties of high-voltage electrical transmission networks, *Electric Power System Research*, vol. 77, pp. 99-105, 2007.

Sabidussi, G., The centrality index of graphs, *Psychometrika*, 31(4), 581-603, 1966.

Schrijver, C.J. and Mitchell, S.D., Disturbances in the US electric grid associated with geomagnetic activity, *J. Space Weather and Space Climate*, 3, A19, 2013.

Silverman, S.M. and Cliver, E.W., "Low-latitude auroras: the magnetic storm of 14-15 may 1921", *Journal of Atmospheric and Solar-Terrestrial Physics*, Vol.63, 523-535, 2001.

Solarstorms, http://www.solarstorms.org. Accessed on 22st October 2014.

Statistics Finland: http://www.stat.fi. Accessed on 6th November 2014.

SWPC, Space Weather Prediction Center: http://www.swpc.noaa.gov/info/Kindex.html. Accessed on 22nd October 2014.

Stephenson, K.A., and Zelen, M., Rethinking centrality: Methods and examples, *Social Networks*, 11, 1–37, 1989.

Strogatz, S. H., Exploring complex networks, *Nature*, Vol. 410, 268-276, 2001.

Thomson, A.W.P., McKay, A. J. and Viljanen, A., A review of progress in modelling induced geoelectric and geomagnetic fields with special regard to geomagnetically induced currents, *Acta Geophysica*, Vol. 57, No. 1, 209-219, 2009.

USGS, United States Geological Survey, www.usgs.gov. Accessed on 5th November 2014.

Viljanen, A., Pirjola, R., Wik, M., Adam, A., Pracser, E., Sakharov, Y. and Katkalov, J., Continental scale modeling of geomagnetically induced currents, *Journal of Space Weather and Space Climate*, 2, 2012.

Viljanen, A., Relation of geomagnetically induced currents and local geomagnetic variations, *IEEE Transactions on Power Delivery*, Vol. 13, No. 4, 1285-1290, 1989.

Wallling, R.A., and Khan, A.H., Characteristics of transformer exciting current during geomagnetic disturbances, *IEEE Transactions on Power Delivery*, Vol.6, No.4, 1991.

Wasserman, S., and Faust, K., *Social Networks Analysis*, Cambridge U.P., Cambridge, 1994.

White, G.F., *Natural hazards: local, national and global*. Oxford University Press, New York, p. 288, 1974.

Wik M., Pirjola R., Lundstedt H., Viljanen A., Wintoft P. and Pulkkinen A., Space weather events in July 1982 and October 2003 and the effects of geomagnetically induced currents on Swedish technical systems, *Annales Geophysicae*, 27, 1775 – 1787, 2009.

Zimmerman, R., Social Implications of Infrastructure Network Interactions, *Journal of Urban Technology*, Vol. 8, No. 3, 97-119, 2001.

Zio, E. and Sansavini, G., Modeling interdependent network systems for identifying cascade-safe operating margins, *IEEE Transactions on Reliability*, 60(1), 94-101, 2011.

Zio, E. and Piccinelli, R., Randomized flow model and centrality measure for electrical power transmission network analysis, *Reliability Engineering and System Safety*, Vol. 95, 279-285, 2010.

Zio, E., Sansavini, G., Maja, R. and Marchionni, G., An analytical approach to the safety of road networks, *International Journal of Reliability, Quality and Safety Engineering*, Vol. 15, No. 1, 67 - 76 February 2008.

European Commission
EUR 26914 EN – Joint Research Centre – Institute for the Protection and Security of the Citizen

Title: Space Weather and Power Grids – A Vulnerability Assessment

Authors: Roberta Piccinelli, Elisabeth Krausmann

Luxembourg: Publications Office of the European Union

2014 – 53 pp. – 21.0 x 29.7 cm

EUR – Scientific and Technical Research series – ISSN 1831-9424

ISBN 978-92-79-43971-1

doi:10.2788/20848

LB-NA-26914-EN-N

JRC Mission

As the Commission's in-house science service, the Joint Research Centre's mission is to provide EU policies with independent, evidence-based scientific and technical support throughout the whole policy cycle.

Working in close cooperation with policy Directorates-General, the JRC addresses key societal challenges while stimulating innovation through developing new methods, tools and standards, and sharing its know-how with the Member States, the scientific community and international partners.

Serving society
Stimulating innovation
Supporting legislation

doi:10.2788/20848

ISBN 978-92-79-43971-1

Publications Office